3

Intracellular recording

Romain Brette and Alain Destexhe

3.1 Introduction

Intracellular recording is the measurement of voltage or current across the membrane of a cell. It typically involves an electrode inserted in the cell and a reference electrode outside the cell. The electrodes are connected to an amplifier to measure the membrane potential, possibly in response to a current injected through the intracellular electrode (current clamp), or the current flowing through the intracellular electrode when the membrane potential is held at a fixed value (voltage clamp). Ionic and synaptic conductances can be measured indirectly with these two basic recording modes. While spike trains can be recorded with extracellular electrodes (see chapter 4 in this book), subthreshold events in single neurons can only be recorded with intracellular electrodes. Intracellular recordings have been used for many applications: measuring membrane potential distribution in vivo (DeWeese et al., 2003), membrane potential correlations between neurons (Lampl et al., 1999), changes in effective membrane time constant with network activity (Pare et al., 1998; Leger et al., 2005), excitatory and inhibitory synaptic conductances in response to visual stimulation (Borg-Graham et al., 1998; Monier et al., 2003; Anderson et al., 2000), current-voltage relationships during spiking activity (Badel et al., 2008), the reproducibility of neuron responses (Mainen and Sejnowski, 1995) dendritic computation mechanisms (Stuart et al., 1999), gating mechanisms in thalamocortical circuits (Bal and McCormick, 1996), oscillations of membrane potential (Volgushev et al., 2002; Engel et al., 2001), stimulus-dependent modulation of the spike threshold (Azouz and Gray, 1999; Wilent and Contreras, 2005; Henze and Buzsaki, 2001), and many others.

We start by a brief historical overview of intracellular recording before describing the main techniques. In this chapter, we explain how to interpret

intracellular measurements of potential, current and conductance and we emphasize the artefacts, uncertainties and limitations of those recording techniques. We do not provide practical details about fabrication and use of electrodes and amplifiers, and we invite the interested reader to refer to specialized books such as (Purves, 1981; Sherman-Gold, 1993) and Chapter 2 in this book.

3.1.1 A brief history of intracellular recording techniques

Many discoveries in neuroscience have been triggered by the development of new tools. Figure 3.1 shows a panel of historical electrophysiological techniques developed over the last two centuries.

Animal electricity. Electrophysiology started at the end of the 18th century when Luigi Galvani observed that the frog muscle contracted when the leg nerve and the muscle were connected through a metal conductor (Galvani, 1791). He concluded that "animal electricity" was present in the nerve and muscle and that the contraction was induced by the flow of electricity through the conductor. That discovery led to the development of the electric battery by Alessandro Volta in 1800. In the next decades (around 1840), Carlo Matteucci observed an outward current flow between the axial cut of a nerve and the undamaged surface using a galvanometer, thus showing the existence of the resting membrane potential. Inspired by Matteucci's work, Emil du Bois-Reymond later discovered the action potential by observing that the outward current was temporarily reduced during electrically induced muscle contraction. His instrument is shown on Fig. 3.1A, it consisted of two electrodes applied on the muscle and connected to a galvanometer.

The first electrophysiological instrument. The galvanometer could not record the time course of action potentials, but his student Julius Bernstein designed an ingenious device called the "differential rheotome" (Fig. 3.1B): one pin on a rotating wheel closes the stimulus circuit when it touches a copper wire, while two other pins on the opposite side of the wheel close the recording circuit (a galvanometer) when passing through a mercury surface. By adjusting the position of the pins, Bernstein was able to sample the electrical response at precise times after the stimulus, and he used his instrument to produce the first recording of an action potential in 1868 (Bernstein, 1868) (Fig. 3.1C). Bernstein's differential rheotome can thus be considered as the first instrument in electrophysiology. He then developed an influential theory according to which the negative resting potential is due to the membrane being permeable to potassium ions and the action poten-

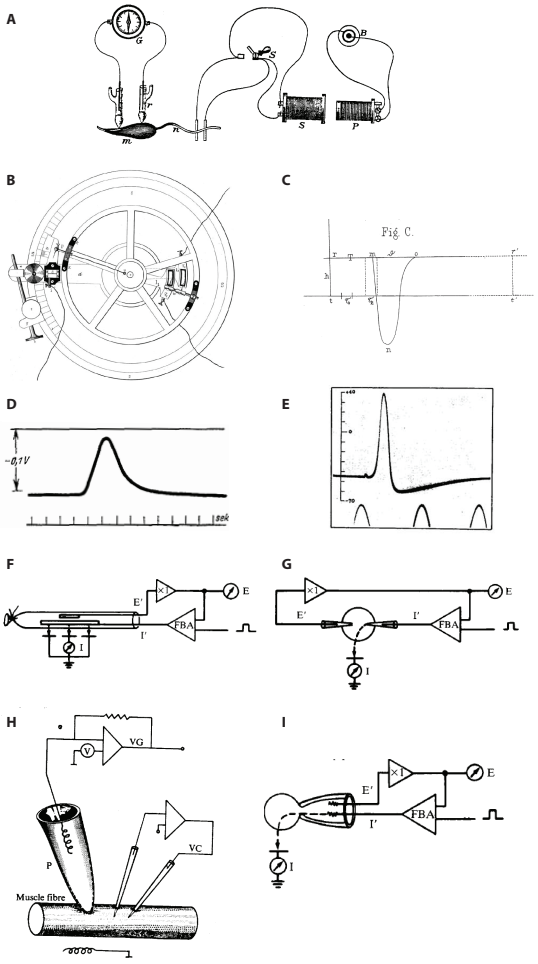

Fig. 3.1. Historical electrophysiological recording techniques. A. Device used by Emil du Bois-Reymond to detect electrically triggered action potentials (APs) in a muscle (1840s). B. Bernstein's differential rheotome (1860s). The rotating wheel samples the electrical response of the muscle at a specific time following electrical stimulation. C. First (extracellular) recording of an AP, using the differential rheotome (Bernstein, 1868). D. First intracellular recording of an AP in a plant cell (Nitellia) by Umrath (1930). Each tick is a second (APs are much slower in plants than in animals). E. First intracellular recording of an AP in an animal cell, the giant squid axon, by Hodgkin and Huxley (1939). F. Voltage clamp setup in the squid axon, designed by Marmont and Cole in 1949 (illustration from Hille (2001)). G. Two-electrode voltage clamp with sharp intracellular electrodes. H. The patch clamp technique, designed by Neher and Sakmann (1976). The transmembrane current is recorded with the large patch electode while the membrane potential is held fixed with two conventional microelectrodes. I. Whole-cell patch clamp (1980; illustration from Hille (2001)). A gigaseal is formed by suction and the membrane is ruptured to give direct access to the intracellular potential.

tial to a non-selective increase in membrane permeability (Bernstein, 1912). For many years, the application of external electrodes was the only available technique for measuring potentials and Bernstein's hypothesis remained unchallenged.

The first intracellular recording. In 1939, Cole and Curtis designed a clever experiment using extracellular electrodes on squid axons and found that the membrane resistance dropped during the action potential (Cole and Curtis, 1939), as predicted by Bernstein's theory. But around the same time, Hodgkin and Huxley managed to insert a glass microelectrode into a squid axon and made the first intracellular recording of an action potential in an animal cell (Hodgkin and Huxley, 1939) (Fig. 3.1E) (the first intracellular recording of an action potential was in fact made by Umrath in 1930 in plant cells (Umrath, 1930); Fig. 3.1D). They found that the intracellular membrane potential becomes significantly positive during the action potential, contradicting Bersntein's theory and leading to the finding that the action potential reflected a selective increase in sodium permeability (Hodgkin and Katz, 1949). Intracellular recordings in vertebrates were performed a few years later, in 1951 (Brock et al., 1952).

The voltage clamp. Because of the explosive character of the action potential, measuring the membrane current-voltage properties that were responsible for the action potential required a new experimental device. At the end of the 1940s, Marmont and Cole designed an electronic feedback system that was able to "clamp" the membrane potential at a fixed value along the squid axon and to measure the feedback current: the voltage clamp (Marmont, 1949; Cole, 1949) (Fig. 3.1F). They were shortly followed by Hodgkin and Huxley, who used that recording technique to develop their quantitative theory of the action potential based on voltage-dependent ionic currents (Hodgkin and Huxley, 1952), for which they were awarded the Nobel Prize for physiology or medicine in 1963. Mammalian cells, which are smaller than giant squid axons, became accessible to intracellular recordings with the development of pulled glass microelectrodes by Ling and Gerard in 1949 (Ling and Gerard, 1949). These electrodes have a sharp tip that can penetrate the membrane with little damage (hence the usual name "sharp electrodes") and are still used today, with minor modifications (Fig. 3.1G).

The patch clamp. Voltage clamping required two electrodes: one for injecting the current and another one for monitoring the voltage, which was technically difficult in small cells. In the 1970s, Brennecke and Lindemann developed a system to alternate current injection and voltage recording on the same electrode (Brennecke and Lindemann, 1971), now called the "discontinuous current clamp", and they showed that it could be used to perform

a single-electrode voltage clamp (now called "discontinuous voltage clamp"). Around the same time, Neher and Sakmann developed a technique to record currents flowing through single ionic channels, by applying the tip of a glass pipette on the surface of the membrane: the patch clamp (Neher and Sakmann, 1976) (Fig. 3.1H). Traditional microelectrodes were still required for voltage clamping the membrane (the two electrodes on the right in Fig. 3.1H) and recording quality was limited by the background noise due to the seal between the patch and the electrode. The technique was refined in 1980 by Sigworth and Neher with the introduction of the "giga-seal" (Sigworth and Neher, 1980), which is a tight contact between patch and electrode with very high resistance (10-100 GΩ), allowing voltage clamping with the same electrode and low noise recordings. Several variations of the patch clamp method were then developed, in particular the "whole-cell" recording, in which the membrane is ruptured to make intracellular recordings in a similar way as with conventional sharp microelectrodes, but with lower access resistance and noise level (Fig. 3.1I). Neher and Sakmann were awarded the Nobel Prize in 1991 for their discoveries.

3.1.2 Experimental setups

A typical setup for intracellular recording consists of a reference electrode (immersed in the bath for slice recordings or possibly in the musculature for recordings *in vivo*) and an intracellular microelectrode, both connected to an electronic amplifier (Fig. 3.2A). The role of the amplifier is to measure the potential of the microelectrode (relative to the reference electrode) and/or to inject currents, while matching input/output impedances (since neuronal signals are typically very small). In some cases, one intracellular electrode is used to monitor the potential and another one to inject currents into the neuron (double-electrode configuration). The amplifier is connected to various electronic devices (e.g. an oscilloscope) and in general to a computer which records the measurements and possibly send commands (e.g. current injection).

3.1.2.1 Electrodes

Intracellular electrodes are thin glass pipettes filled with an electrolyte solution (usually KCl). The tip of the pipette is in continuity with the inside of the cell, while the other end contains a metal wire (usually silver, coated with a composite of silver and silver-chloride) connected to the amplifier (Fig. 3.2B,C). The electrode *per se* is in fact the junction between the elec-

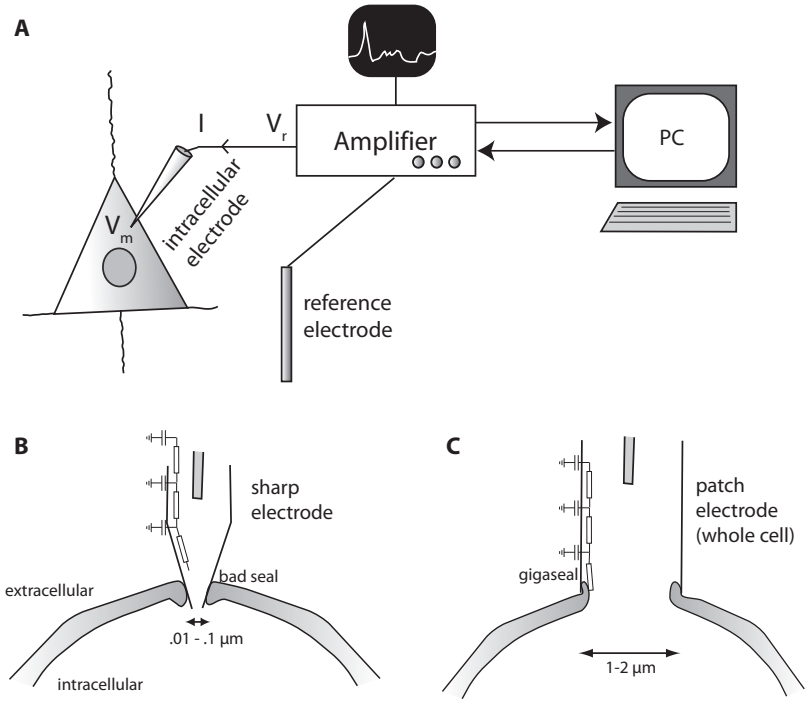

Fig. 3.2. Experimental setups. A. An intracellular electrode is impaled into the cell and connected to an amplifier, which compares its potential with that of a reference electrode. The amplifier output is typically connected to an oscilloscope (top) and computer (right). B. Sharp electrodes have a small tip (equivalent electrical circuit superimposed on the left side of the electrode). C. Patch electrodes have a larger tip, with a better seal with the membrane.

trolyte and the wire, where electrons are exchanged for ions through the following reversible reaction:

$$\mathrm{Cl}^- + \mathrm{Ag} \rightleftharpoons \mathrm{AgCl} + \mathrm{e}^-$$

There are two types of intracellular electrodes: sharp electrodes and patch electrodes (Fig. 3.2B). *Sharp electrodes* (standard intracellular microelectrodes introduced by Ling and Gerard (1949)) are made from pulling a glass capillary tube (diameter ≈ 1 mm), resulting in a very fine tip ($0.01 - 0.1\mu$m) which can penetrate the membrane of the cell (Fig. 3.2B). *Patch electrodes* were initially developed by Neher and Sakmann (1976) for recording currents through small membrane patches containing few channels (hence the name). They are glass tubes with a wide round tip (1-2 μm) which are applied on the surface of the membrane (Fig. 3.2C). A small suction creates a high-resistance seal (> 10 GΩ) between the electrode tip and the membrane.

In that original configuration, one can record the current flowing through a single ionic channel. If pressure is applied through the electrode, the membrane is ruptured and the electrode accesses the inside of the cell: this is called the *whole cell* configuration. In this chapter, we will not describe single channel recording but only intracellular recording — i.e., the whole cell configuration. We suggest the interested reader to refer to (Sakmann and Neher, 1995) for detailed information about single channel recording.

The differences between sharp and patch recordings are summarized in Table 3.1, and result essentially from the difference in tip geometry (thin vs. wide) and in seal quality (bad seal vs. good seal). Electrodes have a resistance, which is the sum of the resistance of the electrolyte solution and of the junction of the cell and electrode. Because sharp electrodes have a thin tip, they usually have higher resistance than patch electrodes, which have a wider tip (although they have a thinner tip and higher resistance when used on thin processes such as dendrites). Junction potentials appear in both types of electrodes and produce offsets in the potential measurement (see section 3.2.2.1). Sharp electrodes have an additional type of junction potential named *tip potential*, which is hard to predict. A thinner tip also implies higher level of noise and more nonlinearities (Purves, 1981). Besides, the seal between a sharp electrode and the membrane is bad, which introduces an additional leak current. On the other hand, patch electrodes are technically more difficult to use, especially for adult animals *in vivo*. More importantly, because the tip is wide, the electrode *dialyses* the cell, that is, the electrolyte solution diffuses into the cell and slowly replaces the soluble contents of the cell's interior.

3.1.2.2 Amplifiers

The role of an electrophysiological amplifier is to measure currents or potentials and to inject currents through the electrode. It includes a number of circuits to minimize noise and various artifacts. In particular, all amplifiers include a circuit to compensate for the input capacitance (capacitance neutralization) and for the electrode resistance (electrode compensation or series resistance compensation circuits). Electrophysiological amplifiers have two recording modes: current clamp and voltage clamp. In current clamp mode, the current flowing from the amplifier is held fixed; in voltage clamp mode, the potential at the amplifier input is held fixed (using a feedback circuit). When two intracellular electrodes are used (in addition to the reference electrode), one electrode injects a current and the other one measures the potential. When only one intracellular electrode is used, the injected current biases the measured potential, as explained below. This is compensated ei-

	Sharp	Patch
Tip geometry	thin	wide
Resistance	**high** (25-125 MΩ)	low in vitro (< 20 MΩ), **higher in vivo** (up to 200 MΩ)
Tip potential	**variable**	negligible
Noise	**high**	low
Seal	**bad**	good
Nonlinearity	**often nonlinear**	generally linear
Dialysis	no	**yes**
Difficulty	easy	**harder** (esp. adults)

Table 3.1. *Properties of intracellular electrodes: sharp microelectrodes and patch electrodes (whole-cell configuration). We highlighted the issues raised by each type of electrode: sharp electrodes have high resistance, variable tip potential (hard to predict), higher noise, often nonlinear behavior and the seal with the membrane is bad (introducing an additional leak current); patch electrodes have high resistance in vivo and in dendrites, they replace the contents of the cell (dialysis) and they are technically more difficult to use (especially in adult animals).*

ther by modifying the measured potential (current clamp) or modifying the voltage command (voltage clamp).

We chose to divide this chapter in sections corresponding to the quantity being measured: voltage, current or conductance. Recording the membrane potential is done in current clamp mode, currents are recorded in voltage clamp mode, and conductance recordings use various indirect techniques. Many figures in this chapter are based on numerical simulations which are explained in more details in the appendix.

3.2 Recording the membrane potential

3.2.1 The ideal current clamp

In an ideal current clamp recording, a current I is injected into the cell through an electrode with negligible resistance, while the membrane potential is recorded (Fig. 3.3A). The membrane potential (voltage difference between the inside and the outside of the cell) is measured by comparing the potential at the amplifier end of the intracellular electrode with the potential of a reference electrode (outside of the cell). If the intracellular electrode has zero resistance and junction potentials are neglected, then the measured potential V_r equals the membrane potential V_m. The response of an isopotential neuron to an ideal current clamp injection $I(t)$ is described

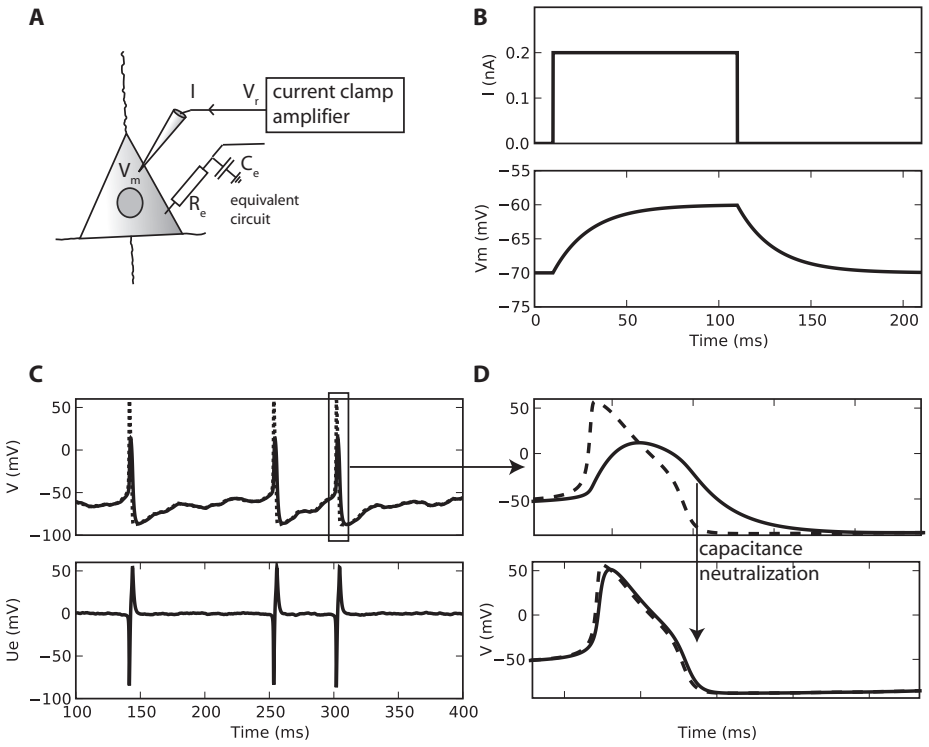

Fig. 3.3. Current clamp recording (numerical simulations). A. Experimental setup: a current clamp amplifier (voltage follower) records the electrode potential (V_r) while injecting a current I through the electrode. Ideally, the recorded potential equals the membrane potential V_m but the electrode resistance (R_e) and capacitance (C_e) introduce artifacts. B. Ideal recorded response to a current pulse, when the electrode resistance is negligible (top: injected current, bottom: recorded potential). C. Recording spontaneous activity with a non ideal electrode: spikes are low pass filtered (top; dashed line: membrane potential, solid line: recording) because a voltage drop develops through the electrode during those fast events (bottom). D. Zoom on an action potential (top). The filtering is reduced with capacitance neutralization (effectively reducing C_e).

by the following differential equation:

$$C\frac{dV_m}{dt} = \sum_{\text{ionic currents}} I_{\text{ionic current}} + I(t)$$

where C is the total membrane capacitance of the neuron (Fig. 3.3B). Measuring the membrane potential without injecting current (i.e., spontaneous activity) is also called a current clamp recording — referring to the fact that a null electrode current is imposed.

Real current clamp recordings differ from this idealized description in a number of ways, even when only spontaneous activity is recorded (no current injection): junction potentials develop at the interface between the electrolyte and the intracellular medium, the electrode is non ideal and filters the signals (both the measured potential and the injected current), sharp electrodes damage the membrane and patch electrodes affect the ionic composition of the intracellular medium. Besides, when current is injected through an electrode with a non-zero resistance, a voltage drop appears between the two ends of the electrode $U_e = V_r - V_m$. That voltage drop must be cancelled, or a second intracellular electrode must be used to measure the membrane potential. We first describe the artifacts that appear when no current is injected, i.e., when measuring spontaneous activity, then we describe the issues arising from current injection through the electrode.

3.2.2 Measuring spontaneous activity

3.2.2.1 Junction potentials

Voltage offsets of different origins arise in intracellular recordings, mostly amplifier input offsets and junction potentials, which occur wherever dissimilar conductors are in contact. The largest junction potentials occur at the liquid-metal junction formed where the wire from the amplifier input contacts the electrolyte in the micropipette and at the liquid-liquid junction formed at the tip the micropipette, called the *liquid junction potential* (LJP). A LJP develops when two solutions of different concentrations are in contact: the more concentrated solution diffuses into the less concentrated one, and a potential develops when anions and cations diffuse at different rates. To suppress this unwanted bias, one usually starts by *zeroing* the measured potential in the bath (outside the cell, before impalement), i.e., a DC voltage offset is added so as to compensate for all voltage offsets. When the electrode accesses the interior of the cell, the LJP changes because the solution around the electrode tip changes, but all other offsets are unchanged. Thus the measured potential is $V_m + V_{\mathrm{LJP}}^{\mathrm{cell}} - V_{\mathrm{LJP}}^{\mathrm{bath}}$, where $V_{\mathrm{LJP}}^{\mathrm{cell}}$ is the LJP between the cell and the electrode solution and $V_{\mathrm{LJP}}^{\mathrm{bath}}$ is the LJP between the bath and the electrode solution. Because the concentrations of the bath and electrode solutions are known, V_{bath} can be calculated (using Henderson equation, see e.g. (Sakmann and Neher, 1995)). With patch electrodes, the LJP between the cell and the electrode vanishes after some time and can thus be neglected. With sharp electrodes, it is very difficult to compensate for the junction potentials because, in addition to the liquid junction

potential, a tip potential develops at the cell/electrode interface because the electrode tip is very thin (Purves, 1981). This tip potential is unfortunately difficult to predict with precision.

3.2.2.2 Damages induced by the electrode

Sharp microelectrodes have a very fine tip (0.01 – 0.01μm) which perforates the membrane of the cell. Thus, the membrane is damaged when the electrode impales the neuron. In particular, a leak appears because of the bad quality of the seal between the electrode and the membrane. It can be modelled as an outward current $I_{\text{leak}} = -gV_m$, where g is the conductance of that leak. The total conductance of the neuron is thus increased when the electrode perforates the membrane, so that the effective membrane time constant $\tau_m = C/g_{\text{total}}$ is decreased. This effect explains why the membrane time constant is larger and the resting potential is lower when measured with patch electrodes (whole-cell configuration) than when measured with sharp electrodes (Staley et al., 1992).

Patch electrodes do not suffer from the same problem because the electrode tip is sealed to the membrane with a "gigaseal" (resistance 10–100 GΩ). However, because the tip is wide (1 – 2μm) and the volume of the electrode is much larger than the volume of the cell, the electrolyte solution diffuses into the cell and slowly replaces the soluble contents of the cell's interior, which can alter the properties of the cell over time ($>$ 10 minutes). This phenomenon is referred to as the electrode *dialyzing* the cell. To avoid dialysis, a variant of the whole-cell configuration has been developed: the perforated patch clamp. In this configuration, instead of rupturing the membrane, the experimenter adds an antibiotic to the electrode solution, which makes small perforations in the membrane patch at the tip of the electrode. That technique prevents the dialysis but it also increases the access resistance and the recording noise.

3.2.2.3 Electrode filtering

Real electrodes have a non-null resistance, which is the sum of the resistance of the electrolyte solution and of the junction of the cell and electrode. The electrode resistance is thus more precisely referred to as the *access resistance*. If the electrode were a pure resistor, it would not affect the measurement (when no current is injected) since no current would pass through it, so that $V_r = V_m$. Unfortunately, the electrode and amplifier input have a capacitance: the *input capacitance*, on the amplifier side, and a distributed wall capacitance along the glass tube of the electrode. As a result, current can flow through the electrode and bias the potential measurement: $V_r \neq$

V_m. As a first approximation, the electrode can be modelled as a resistor R_e and input capacitance C_e on the amplifier side. It follows that the electrode acts as a first-order low pass filter with cut-off frequency $f_c = 1/(2\pi R_e C_e)$. The quantity $\tau_e = R_e C_e$ is the *electrode time constant*. Electrode filtering has a very significant effect on the recording of fast phenomena such as action potentials, which appear wider and smaller than they are in reality at the recording site, as shown on Fig. 3.3C,D. Thus, reliable measures of action potential width and height depend crucially on the correction of the electrode capacitance.

To reduce this problem, modern electrophysiological amplifiers include a *capacitance neutralization* circuit, which compensates for the input capacitance by an electronic feedback circuit. The current flowing through the input capacitance is $C_i dV_r/dt$; capacitance neutralization consists in inserting a "negative capacitance", that is, adding the opposite current $-C_i dV_r/dt$ to cancel the capacitive current. Since the precise value of the capacitance is unknown, it is manually adjusted by turning a knob on the amplifier, so that the actual compensating current is $-C^* dV_r/dt$. When $C^* > C_i$, the circuit becomes unstable, which can damage the cell. Tuning the capacitance neutralization circuit therefore requires careful adjustment. In reality, the capacitance can never be totally compensated because this feedback circuit can only cancel the capacitive current at the amplifier end of the electrode, but not the distributed capacitance along the glass tube of the electrode. Therefore when the input capacitance is completely cancelled, further increasing the capacitance neutralization results in unstability and the total capacitance is never completely suppressed at the optimal point.

This circuit reduces the effective electrode time constant and increases the cut-off frequency of the filtering, but at the same time it increases the level of noise in the recording (which appears very clearly on the oscillope as traces become thicker), for two reasons: electrode filtering masks some of the recording noise, and the capacitance neutralization circuit itself amplifies noise because it is a feedback circuit.

3.2.3 Measuring the response to an injected current

In many cases, the membrane potential response to an injected current is to be measured. This is obviously standard for *in vitro* experiments when one wants to measure neuronal properties, such as the properties of ionic channels, but also *in vivo*, for example to evaluate the effective membrane time constant of a neuron during spontaneous activity by observing the response to current pulses (Pare et al., 1998; Leger et al., 2005). In those

cases, the main issue is that when a current is passed through an electrode with non-zero resistance, a voltage drop U_e appears between the two ends of the electrode, so that $V_r = V_m + U_e$. For a constant current I, this voltage drop is $U_e = R_e I$, where R_e is the electrode resistance (Fig. 3.4). The electrode resistance is inversely correlated with the diameter of the electrode tip (Purves, 1981), so that sharp electrodes typically have high resistance (about 100 MΩ). Patch electrodes have a lower resistance because their tip is wider, although higher-resistance electrodes must be used *in vivo* and when recording in thin processes (dendrites, axons). The electrode resistance depends partially on the interface between the electrode and the cell and thus cannot be reliably estimated before impalement. Besides, it often varies during the course of an experiment. A secondary issue, which is partially solved by capacitance neutralization, is that the injected current is filtered by the electrode.

One way of solving the electrode resistance problem is to use a second, non-injecting, intracellular electrode to measure the membrane potential (although the injected current remains filtered). However, this is technically difficult, especially *in vivo*, and it also increases the cell damage. The alternative solution consists in correcting the measurement bias induced by the electrode. There are essentially three available methods to suppress the electrode voltage during current injection: bridge balance, discontinuous current clamp and active electrode compensation.

3.2.3.1 Bridge balance

As a first approximation, the electrode can be modelled as a pure resistor with resistance R_e, so that the voltage across the electrode during current injection is $U_e = R_e I$ and the recorded potential is $V_r = V_m + R_e I$ (Fig. 3.4A). The membrane potential can thus be recovered from the raw recording by subtracting U_e: $V_m = V_r - R_e I$. This method is named *bridge balance* or *bridge compensation*, in reference to an electrical circuit called the Wheatstone bridge, which was used in old amplifiers to perform that subtraction. Modern electrophysiological amplifiers now use operational amplifiers to perform this operation, but the name has remained. Since the electrode resistance R_e is unknown, it is estimated with an adjustable knob on the amplifier, which is manually tuned by the experimenter. The classical method to determine that resistance is to inject a current pulse into the cell and to ajust the bridge resistance until the recorded potential response "looks correct" in the eye of the experimenter (Fig. 3.4B,C). That adjustment is easy if the electrode is indeed a pure resistor: in that case, the response of the electrode to a square current pulse is also a square pulse

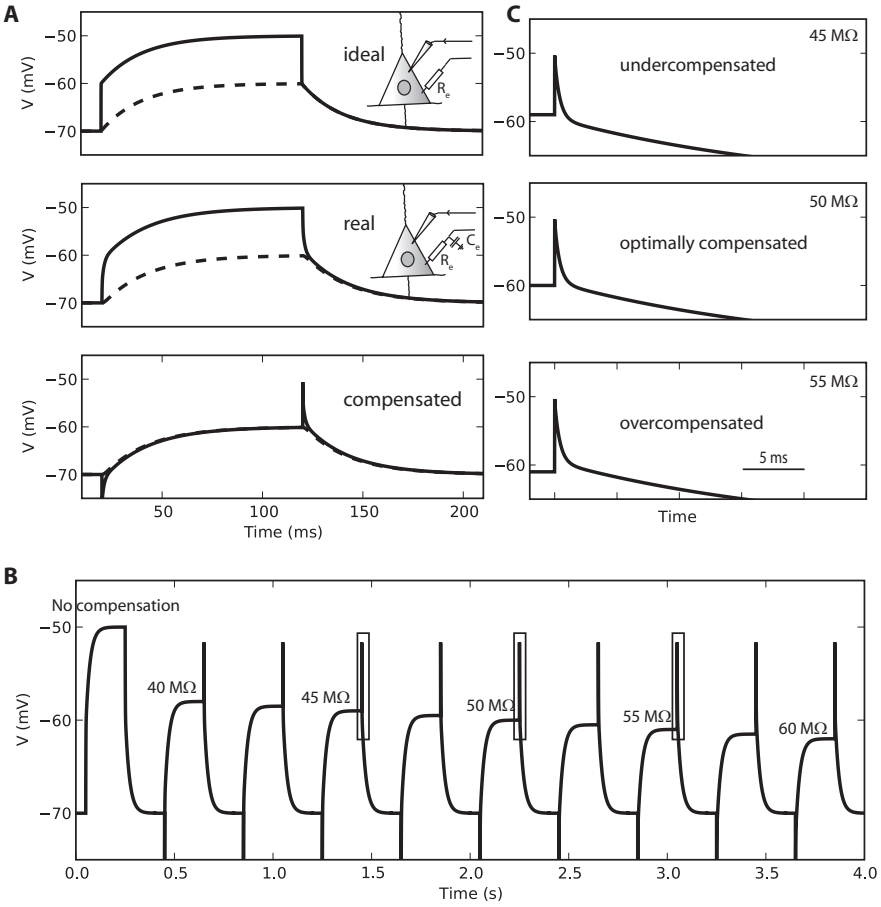

Fig. 3.4. Bridge balance (numerical simulations). A. Membrane potential (V_m, dashed line) and current clamp recording (V_r, solid line) in response to a current pulse. Top: With a purely resistive electrode (resistance R_e) the recorded potential is $V_m + ReI$, with a discontinuity at pulse onset. Middle: a real electrode has a capacitance (C_e), which smoothes the onset. Bottom: bridge balance consists in subtracting R_eI, which produces discontinuities at pulse onset (capacitive transients). B. Manual tuning of bridge balance. The estimated resistance is progressively increased until the trace "looks right" (real resistance: $R_e = 50M\Omega$). The transients in boxes are magnified in C. C. The shape of capacitive transients is used to determine the optimal bridge setting.

(with height R_eI), so that any mismatch in estimated resistance results in a discontinuity (a vertical line on the oscilloscope) at the onset of the pulse. Unfortunately, even when the capacitance neutralization circuit is used, the electrode capacitance is never completely cancelled and the adjustment of

the bridge resistance is more difficult. Because the electrode time constant is non null, the response of the electrode to the onset of a current pulse is approximately exponential:

$$U_e(t) = (1 - e^{-t/\tau_e})R_e I$$

where $\tau_e = R_e C_e$ (C_e is the uncompensated electrode capacitance). bridge balance amounts to subtracting a square pulse from width τ_e, so that the compensated bridge recording is:

$$V_{\text{bridge}} = V_m + (1 - e^{-t/\tau_e})R_e I - R_e I = V_m - e^{-t/\tau_e} R_e I$$

Thus, a negative transient appears at the onset of the pulse, with height $R_e I$ and width τ_e. Since this transient is due to the non zero capacitance of the electrode, it is often called "capacitive transient". Capacitive transients do not constitute a major problem if only constant currents are injected, but they can completely obscure the measured signal when a fast time-varying current is injected.

The finite capacitance of the electrode poses another problem for bridge balance, both for constant and time-varying current injection: it makes the estimation of the electrode resistance more difficult. Indeed, the adjustment of the bridge resistance relies on the discontinuity of the electrode response, which is unambiguous only when $\tau_e << \tau_m$ (τ_m is the membrane time constant). To our knowledge, it is not precisely known what visual cues electrophysiological experimenters implicitly use when manually balancing the bridge in face of that ambiguity. However, it seems that manually estimated resistances approximately agree with those obtained from a simple exponential fitting procedure described in (Anderson et al., 2000), where the recorded response is modelled as

$$V_r(t) = V_0 + (1 - e^{-t/\tau_m})R_m I + (1 - e^{-t/\tau_e})R_e I$$

where V_0 is the resting potential and R_m is the neuron resistance. This formula is the superposition of the cell response to a direct injection of the current and of the response of the electrode alone (i.e., in the bath). Fitting the recording with this expression provides an estimated value of the electrode resistance R_e. This expression is however only an approximation, even if both the membrane and the electrode are RC circuits, because the injected current is filtered before entering the cell and current can also flow from the neuron through the electrode. If the membrane and electrode are modelled as RC circuits, then the response is indeed biexponential but with different coefficients, as described in (de Sa and MacKay, 2001):

$$V_r(t) = V_0 + (ae^{-\mu_1 t} + be^{-\mu_2 t} + c)I$$

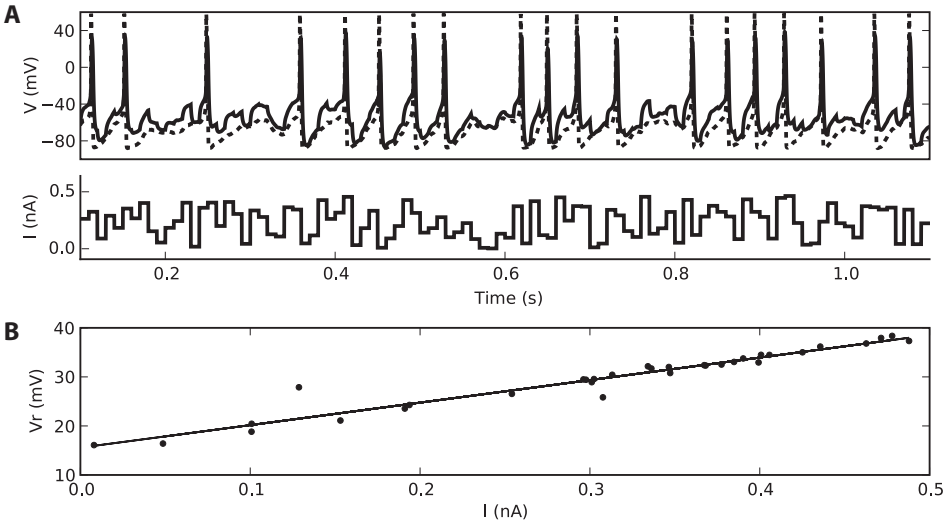

Fig. 3.5. Estimating the electrode resistance (R_e) from spikes (numerical simulations). A. Membrane potential (V_m, dashed line) and (uncompensated) current clamp recording (V_r solid line) in response to a random current injection (bottom). B. The recorded voltage at the peak of action potentials is approximately $V_r = V_m + R_e I$ (dots), where V_m is assumed constant. The slope of the I–V_r relationship is found with linear regression (line) and provides an estimate of R_e: 45 MΩ instead of 50 MΩ (real value).

where the coefficients are related to R_m, R_e, τ_m and τ_e by complex formulae. In general the electrode resistance R_e is not equal to the factor in front of the fastest exponential. The relationship can be inverted and gives:

$$\begin{aligned} C_e &= \frac{1}{\mu_2 c - (\mu_1 - \mu_2)a} \\ R_e &= \frac{1}{C_e(\mu_1 + \mu_2) - cC_e^2\mu_1\mu_2} \\ R_m &= c - R_e \\ C_m &= \frac{1}{\mu_1\mu_2 C_e R_e R_m} \end{aligned}$$

Thus, fitting the recorded response to a pulse to a biexponential function and using the formulae above provides a better way to estimate the electrode resistance for bridge balance. However, the method does not work so well in practice because once the input capacitance has been maximally compensated with the capacitance neutralization circuit of the amplifier, the electrode response is generally not exponential anymore (essentially because the remaining capacitance is distributed along the electrode).

Another way to estimate the electrode resistance is to take advantage of the stereotypical nature of action potentials (as in Anderson et al. (2000)). If the peak voltage of action potentials (APs) is constant, then any measured variability in AP height should be attributed to a mismatch between the bridge and the electrode resistance. Indeed, if V_{peak} is the peak value of APs, then the measured value when current is injected through the electrode should be $V_{\text{bridge}} = V_{\text{peak}} + \Delta R_e I$, where $\Delta R_e = R_e - R_{\text{bridge}}$ is the mismatch between the electrode and bridge resistance. Therefore, the slope of the linear regression between measured values of V_{bridge} and I is the difference between electrode and bridge resistance, i.e., the error in bridge balance (Fig. 3.5). However, this method should be used with caution and only as a check, because the shape of APs can in fact vary as a function of the stimulation: in cortical neurons, it has been observed that AP height is inversely correlated with AP initiation threshold, which is inversely correlated with the slope of the depolarisation preceding the AP (Azouz and Gray, 1999; de Polavieja et al., 2005; Wilent and Contreras, 2005; Henze and Buzsaki, 2001). This property is probably due to the inactivation of sodium channels or to the activation of potassium channels. Thus, injected current and AP height should be positively correlated, which restricts the applicability of this method.

It should thus be kept in mind that in general bridge balance is not straightforward and the resulting compensation is imperfect. Besides, the access resistance can change over time, especially in technically difficult situations such as whole-cell recordings *in vivo*, which can compromise the bridge balance. Finally, sharp electrodes are unfortunately not always linear. Nonlinearities arise from the dissimilarity of solutions at the tip of the electrode (Purves, 1981). The amount of nonlinearity is inversely correlated with the tip diameter, which is inversely correlated with resistance, so that higher resistance electrodes tend to be more nonlinear. Nonlinearities can be minimized by choosing an electrode solution that matches the composition of the intracellular medium.

3.2.3.2 Discontinuous Current Clamp

Before patch-clamp recordings were developed by Neher and Sakmann (Neher and Sakmann, 1976), high resistance sharp microelectrodes were the only tool available for intracellular recording. In the early 1970s, Brennecke and Lindemann introduced a new technique (Brennecke and Lindemann, 1971) to solve the problem of the electrode resistance in current clamp mode, later adapted for voltage clamping (Brennecke and Lindemann, 1974). The technique was called *chopped current clamp* and later *discontinuous current*

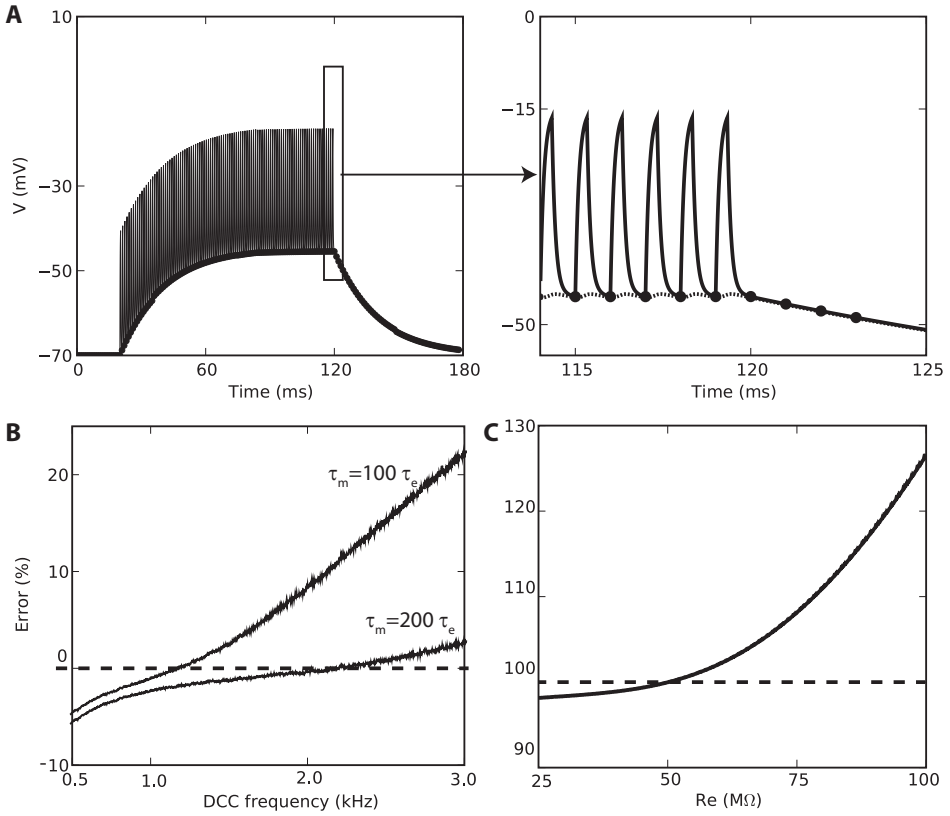

Fig. 3.6. Discontinuous Current Clamp (DCC, numerical simulations). A. Response to a current pulse injection in DCC mode (solid: electrode potential, dashed: membrane potential, dots: sampled recording). Current injection and potential recording are alternated. B. Error in membrane potential as a function of DCC frequency, for a fast electrode ($\tau_m = 200\tau_e$) and for a slower electrode ($\tau_m = 100\tau_e$). A constant current is injected and the depolarization is measured. The measurement is less reliable for the slower electrode. C. Error in membrane potential as a function of electrode resistance (R_e) for the second electrode ($\tau_m = 100\tau_e$), with fixed DCC frequency (optimal frequency for $R_e = 50$ MΩ). This plot shows the effect of a change in electrode resistance during the course of an experiment.

clamp (DCC). The idea is to alternate current passing and voltage measurement so that no current flows through the electrode when the potential is measured (Fig. 3.6A). The alternation rate is determined by the electrode time constant.

In DCC mode, the current command I_{cmd} is sampled at regular intervals Δ. Current is injected through the electrode only during the initial part of each interval. The proportion of time during which current is passed is called

the *duty cycle* and is usually 1/3. During that time, the sampled current is injected through the electrode with the appropriate scaling, so as to conserve the total charge (i.e., $I = 3I_{\text{cmd}}$ if the duty cycle is 1/3). The potential is sampled at the end of each interval, when no current is passed. Since no current is passed during the last 2/3 of the interval, the electrode voltage $U_e(t)$ has decayed approximately as $\exp(-\frac{2\Delta}{3\tau_e})$, which is small if the sampling interval Δ is large compared to the electrode time constant τ_e. In that case, the electrode voltage U_e has vanished when the potential V_r is sampled at the end the interval, so that $V_r \approx V_m$. However, the membrane potential V_m also decays when no current is passed, so that the sampling interval should be short compared to the membrane time constant τ_m. Therefore the sampling interval Δ should be such that $\tau_e << \Delta << \tau_m$, and a reasonable trade-off can be found if τ_e is at least two orders of magnitude shorter than τ_m (Finkel and Redman, 1984).

The optimal sampling frequency. Suppose we want to measure the membrane potential response to a constant injected current I, which should ideally be $V_0 + R_m I$ in the stationary regime, where V_0 is the resting potential and R_m is the membrane resistance. If the sampling frequency is very high, then the sampled potential includes a large residual electrode component, so that the membrane potential is overestimated. As the sampling frequency is made increasingly lower, then the sampled potential tends to the resting potential, i.e., it is underestimated. Thus, there is an intermediate frequency at which the sampled stationary potential is exactly the ideal potential $V_0 + R_m I$. Note however that the real membrane potential is not constantly $V_0 + R_m I$ but it is periodically varying at the DCC sampling period.

But how can that optimal frequency be determined? The standard experimental method is empirical and based on observing the continuous electrode potential on an oscilloscope synchronized to the DCC sampling clock, i.e., the electrophysiologist observes the electrode potential in response to the injected current at the timescale of one DCC period (a fraction of millisecond). The sampling frequency is the highest one such that the observed response at the oscilloscope looks flat, meaning that the electrode response has settled to a stationary value at the end of the duty cycle. One usually makes sure that the DCC setting matches bridge compensated recordings. In other words, that frequency tuning technique consists in adjusting the duty cycle to a few times the electrode time constant τ_e. Given that the duty cycle is 1/3 the sampling period, the sampling period is set at about $10\tau_e$ with that standard technique. Implicitly, it is assumed that the membrane potential

V_m does not significantly change between the two endpoints of the sampling interval, which might be so only if the membrane time constant τ_m is more than several tens of electrode time constants τ_e.

In fact, for any electrode time constant τ_e, there is always an optimal sampling frequency such that the measured stationary voltage is precisely $V_0 + R_m I$. Indeed, that voltage increases continuously with the frequency, is an overestimation at high frequencies and an underestimation at low frequencies. This simple fact would suggest that the use of the DCC technique is not restricted to short electrode time constants. However, there are two practical problems:

- Determining the optimal frequency is not trivial. If one plots the voltage error as a function of the DCC frequency (Fig. 3.6B), the optimal frequency is near the inflexion point of that curve when the ratio τ_m/τ_e is large (> 100), and there is a broad plateau so that a small error in frequency results in a small estimation error. Choosing the inflexion point as the optimal frequency is probably close to the visual procedure with the synchronized oscilloscope that we described above. However, when the ratio τ_m/τ_e is not so large, the frequency – voltage error curve does not have a broad plateau and the optimal frequency is higher than the inflexion point. Thus in that case there is no practical way to determine the optimal frequency and a small error in frequency results in a rather large voltage estimation error.
- The optimal frequency depends on both electrode properties and membrane properties. In particular, setting the optimal frequency at rest can lead to estimation errors during neuronal activity, if the membrane time constant changes.

Noise and artifacts. Besides the problem of setting the sampling frequency, DCC recordings are noisier than bridge recordings for two reasons: sampling the voltage results in aliasing noise (frequencies higher than the sampling frequency add noise at lower frequencies), and capacitance neutralization has to be used at its maximum setting in order to shorten the electrode time constant, which also increases the noise because it is a feedback circuit.

Another artifact is that the input current is distorted. Indeed, during one sampling period, the injected current is 3 times the command current during a third of the sampling interval. Thus, the observed neural response is the response to the command signal with additional high frequencies (harmonics of the DCC frequency). This can potentially lead to artifacts because of the

nonlinear nature of neurons; for example additional high frequencies in the input signal may trigger additional action potentials in the neuron.

Electrode nonlinearities and resistance instabilities. The DCC technique was historically introduced to solve the problem of resistance instability with microelectrodes. Indeed, if the membrane and electrode time constants are well separated, then the measured voltage at the end of the sampling period contains a very small contribution from the electrode, so that changes in electrode properties have minor effects on the measured voltage. Again, this desirable property is conditioned to the fact that the ratio τ_m/τ_e is very large. With reasonable ratios (τ_m/τ_e=100), the optimal DCC frequency corresponds to a point when the electrode voltage does not completely vanish at record times, in order to compensate for the decay in the membrane potential. Thus, an increase in electrode resistance results in overestimation of the membrane potential, but the error remains smaller than with bridge balance (Fig. 3.6C).

Electrode nonlinearities that arise with sharp microelectrodes are typically described as resistance changes as a function of the injected current, which suggests that DCC should reduce the impact of those nonlinearities under the same assumptions (large ratio τ_m/τ_e). However, the extent of this reduction is not so clear because some nonlinearities (type I nonlinearities) are associated with a maximum outward current, which cannot be corrected by the DCC technique (Purves, 1981). Besides, electrode nonlinearities are slow processes while DCC acts on a fast timescale.

3.2.3.3 Active Electrode Compensation

Active Electrode Compensation is a recently introduced technique to compensate for the electrode voltage during single-electrode recordings (Brette et al., 2008). As for the classic bridge balance method, it consists in estimating the voltage drop across the electrode during current injection. The main difference is the electrode model: instead of seeing the electrode as a resistor, it is modelled as an arbitratrily complex circuit of resistances and capacitances, which can be represented by a linear time-invariant filter, i.e., the response of the electrode to a current $I_e(t)$ is expressed as a convolution:

$$U_e(t) = (K_e * I_e)(t) = \int_0^{+\infty} K_e(s) I_e(t-s) ds$$

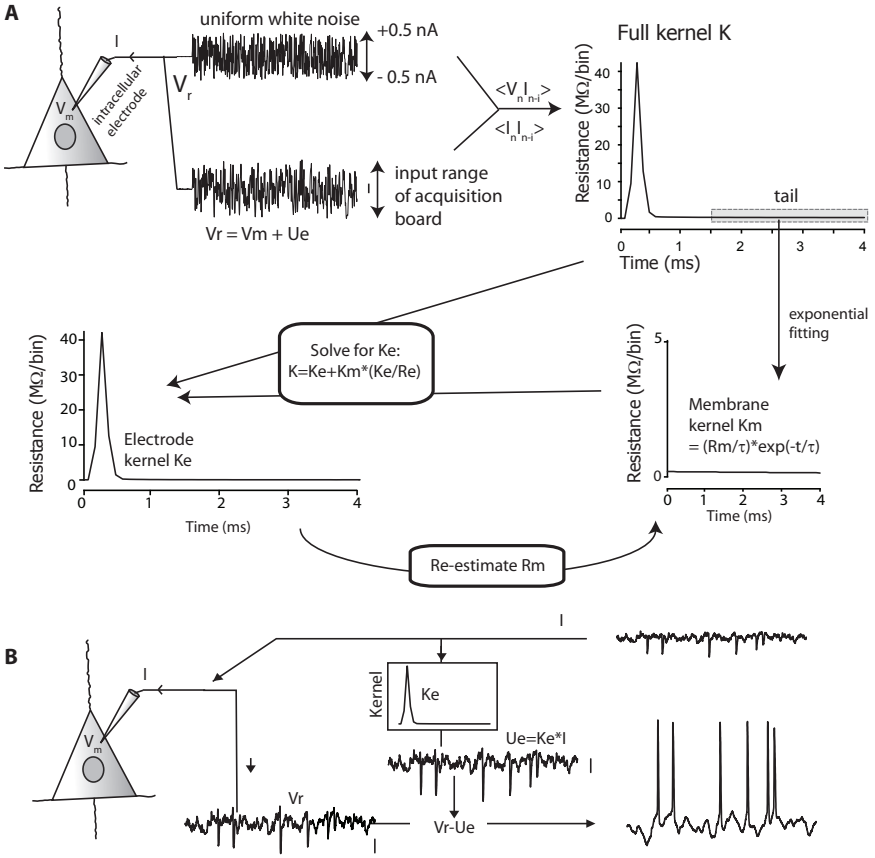

Fig. 3.7. Active Electrode Compensation (AEC). A. A noisy current is injected into the neuron and the total response $V_r = V_m + U_e$ (U_e is the voltage drop through the electrode) is recorded. The cross-correlation between the input current and the output voltage and the autocorrelation of the current give the kernel K (or impulse response) of the neuronal membrane + electrode system (full kernel K, right). The tail of the kernel is fit to an exponential function, which gives a first estimation of the membrane kernel K_m (note: the resistance of each bin is very small since the kernel is distributed over a long duration). The electrode kernel K_e is recovered from K and K_m by solving the equation $K = K_e + K_m * (K_e/R_e)$ (convolution). The process is iterated several times to obtain a better estimation of the membrane kernel. B. Once the electrode kernel has been calibrated, it is then used in real time for electrode compensation: the injected current is convolved with the electrode kernel to provide the electrode response U_e to this current. U_e is then subtracted from the total recorded voltage V_r to yield the estimated V_m.

where K_e is named the *electrode kernel*. In practice, recordings are digitized and the formula reads:

$$U_e(n) = \sum_{0}^{+\infty} K_e(p) I_e(n-p)$$

The technique consists of 1) identifying the electrode kernel by observing the response to a known noisy current and 2) estimating the electrode voltage during current clamp injection and subtracting it from the measured potential (Fig. 3.7). The main difficulty is that the electrode kernel can only be estimated when the electrode impales the neuron (because electrode properties change after impalement). Thus the estimation algorithm consists in 1) finding the kernel of the full system neuron + electrode (+ amplifier) from the voltage response to a known input current and 2) extracting the electrode kernel from the full kernel.

By using small white noise currents, the voltage response of the system is approximately linear and reads in the digital domain:

$$V_n = V_0 + \sum_0^{+\infty} K_p I_{n-p}$$

where V_0 is the resting potential and K is the unknown kernel of the full system (neuron + electrode). Assuming Gaussian noise, the best estimation of K and V_0 is found by solving the linear least-squares problem, as explained in (Brette et al., 2008, 2009). The difficult part, which involves more assumptions, is to extract the electrode kernel K_e for the full kernel K. It is useful to observe that in a linear system, the kernel or impulse response K completely characterizes its responses, so that K is all the information that one can ever obtain about the system using a single-electrode. Therefore, without further assumption, there is no way to separate the membrane and the electrode contributions. The full kernel K can be approximated as $K = K_m + K_e$, where K_m is the membrane kernel, but this is a poor approximation because the injected current is filtered by the electrode before entering the neuron, so that a better approximation is:

$$K = K_m * \frac{K_e}{R_e} + K_e \tag{3.1}$$

where $R_e = \int K_e$ is the electrode resistance. If K_m is known, that convolution equation can be solved by various methods, for example by using the Z-transform or by expressing it as a linear system were the unknowns are the vector components of K_e. Unfortunately K_m is unknown so that further assumptions are required. In the AEC technique, two assumptions are then made:

- The electrode is faster than the membrane, i.e., its electrode kernel vanishes before the membrane one.
- The membrane kernel is that of a first-order low pass filter (an exponential

function), so that it can be parameterized by the (unknown) membrane resistance R_m and the membrane time constant τ_m.

For every value of (R_m, τ_m) there is a solution to the convolution equation (3.1). The first assumption means that we are looking for the solution K_e with the smallest tail (i.e., minimizing $\int_T^{+\infty} K_e^2$, where T is the expected duration of the electrode kernel), which involves an optimization algorithm.

There are 3 main difficulties and limitations with the AEC technique:

Ratio of time constants: Equation (3.1) is a good approximation when the electrode time constant is significantly shorter than the membrane time constant. The quality of electrode kernel estimation degrades with larger ratios τ_e/τ_m: as a rule of thumb, the error in signal reconstruction grows as τ_e/τ_m. Empirically, the method is useful when the electrode time constant is about one order of magnitude shorter than the membrane time constant, which is better than with DCC (two orders of magnitude). bridge balance also requires a good separation of time constants in order to estimate the bridge resistance. As we mentioned previously, because the full kernel K is the only information available in single-electrode recordings, there is no way to distinguish between electrode and membrane kernel if they act on the same timescale.

Dendrites: To extract the electrode kernel from the full kernel, an assumption (i.e., a model) has to be made about the membrane kernel K_m. In the AEC technique, K_m is modelled as a single exponential function, which amounts to seeing the neuron as a sphere with no dendrites. When the dendritic tree is taken into account, the kernel includes additional faster exponential functions, some of which can have similar time constants to the electrode kernel. In this case, these additional functions due to the dendrites are mistakenly included in the estimated electrode kernel, leading to an overestimation of the electrode resistance R_e. The magnitude of the resulting error depends on the geometry of the cell and the recording point (soma or dendrite). In somatic recordings of cortical pyramidal cells, that error was found to be small (Brette et al., 2008) (using numerical simulations of morphologically reconstructed cells). It could be larger when recording in thin processes such as dendrites or axons. In that case, a different model for K_m could be used (Brette and Destexhe, work in progress).

Electrode nonlinearities: The central assumption of the AEC technique is that the electrode is linear. This is not always the case of sharp mi-

croelectrodes, which can show current-dependent resistance changes. Physical modeling of nonlinearities (Purves, 1981) indicates that these are slow processes due to redistribution of ions near the electrode tip. Nonlinearities are stronger for electrode tips with a small radius (which is inversely correlated with the resistance) and when the concentrations of the two solutions (intracellular and inside the electrode) differ. However in practice the amount of electrode nonlinearity is highly variable and unfortunately cannot be assessed before the electrode is impaled into the cell — although electrodes with an unusually high resistance in the slice can be discarded from the start. This nonlinearity problem is not different with AEC than with standard bridge balance, however AEC provides a simple way to measure it, and possibly discard the recordings if the nonlinearity is too important. Electrode nonlinearities are usually measured before impalement from the I-V curve of the electrode, but it is not possible to use the same approach intracellularly because the I-V curve of the electrode could be confused with the I-V curve of the neuron. AEC can be used to measure the electrode resistance by running the kernel estimation procedure intracellularly with different levels of constant injected current, corresponding to the typical (average) levels that will be used subsequently, and check that the amount of nonlinearity is acceptable (in the experiments in (Brette et al., 2008), about half the electrodes were not significantly nonlinear).

3.3 Recording currents

3.3.1 The ideal voltage clamp

In an ideal voltage clamp recording, the membrane potential of the cell is held at fixed value V_{clamp} while one measures the current flowing through the electrode. Assuming an isopential neuron with an ideal voltage clamp setup, the membrane potential is constant ($V_m = V_{\text{clamp}}$) and its derivative is null, so that:

$$0 = \sum_{\text{ionic currents}} I_{\text{ionic current}} + I(t) \tag{3.2}$$

where $I(t)$ is the current flowing through the electrode. Thus, the voltage clamp configuration is used to measure ionic currents flowing when the membrane is held at a given potential. For this reason, the reported voltage clamp current is generally $-I(t)$, the opposite of the current through the

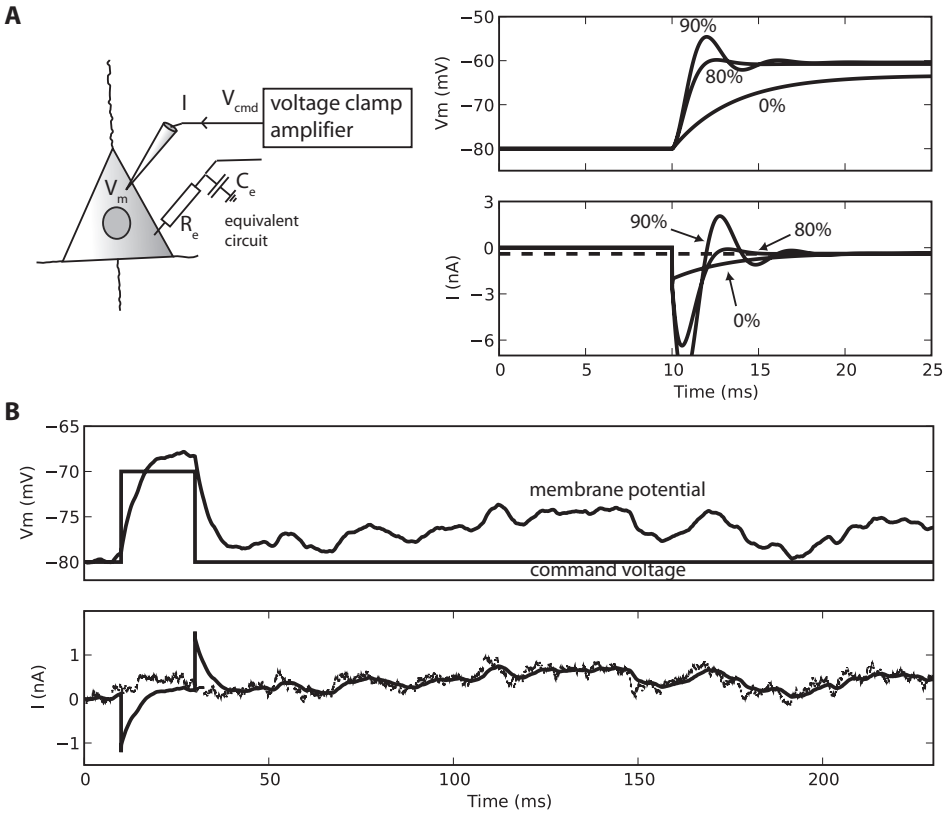

Fig. 3.8. Voltage clamp (numerical simulations). A. In a passive neuron (only leak current), the voltage command is set at -60 mV at time $t = 10$ ms and the actual membrane potential response is shown (top) together with the measured current (bottom; dashed line: ideal measured current). When the electrode resistance is not compensated (0%), the response is slow and does not reach the command potential. The settling time and the clamp error are reduced with compensation (80%) but the resistance cannot be completely compensated because of capacitive effects, inducing oscillatory instability (90%). B. The neuron receives a noisy excitatory synaptic current (bottom, dashed) and is measured in voltage clamp with offline compensation (bottom, solid). A square voltage pulse (top) is used to estimate R_e, then the command voltage is -80 mV. The estimated resistance is $\Delta V/\Delta I$ (ΔI is the current discontinuity, bottom). Offline compensation corrects the error in the mean current but not the high-frequency components.

electrode. In a typical voltage clamp experiment, the clamp potential is instantaneously switched from a resting value to a target value (step change) and transient currents from voltage-dependent channels are measured. In that case, the speed of clamping is an important issue (i.e., how fast the membrane potential follows the command potential). In other experiments

(essentially *in vivo*), the voltage is held fixed and time-dependent changes in currents, typically resulting from synaptic activity, are measured. In both types of experiments, the two main issues are the quality of membrane potential clamping (the difference between V_m and V_{clamp}) and the quality of current recording (Fig. 3.8).

The voltage clamp is implemented as a negative feedback circuit (either analog or digital): the clamp error $V_m - V_{\text{clamp}}$ is measured and a feedback current is injected, such as $I = g(V_{\text{clamp}} - V_m)$, where g is a large (ideally infinite) gain. One can see that when the system is stabilized (implying $dV_m/dt = 0$), the injected current I necessarily satisfies equation (3.2). There are a number of difficulties with this technique:

- The neuron potential can be clamped at only one point: the soma may be clamped at a given potential while remote dendritic locations are not. This is a problem when recording currents originating from dendrites and is called the *space clamp* problem.
- The membrane potential needs to be measured, which requires an electrode compensation technique if there is a single electrode. Because compensation errors can destabilize the system, it is common that only partial electrode compensation be applied.
- Because of various capacitive currents and imperfections, the feedback gain cannot be made arbitrarily large without destabilizing the system. Lower feedback gains result in an imperfect clamp ($V_m \neq V_{\text{clamp}}$).

In modern amplifiers, an additional control feedback is inserted to ensure that the membrane potential is clamped at the correct value: $I = g(V_{\text{clamp}} - V_m) + I_c$, where the control current I_c is proportional to the integral of the clamp error, i.e.:

$$\frac{dI_c}{dt} = g_c(V_{\text{clamp}} - V_m)$$

where g_c is another gain parameter (in units of conductance per time). This is called a *proportional-integral controller* (PI) in control engineering. When the system is stationary, the equality $dI_c/dt = 0$ implies that the membrane potential is clamped at the correct value $V_{\text{clamp}} - V_m$ (assuming that there is no error on measuring the membrane potential V_m).

3.3.1.1 Space clamp issues

In principle, the membrane potential can only be imposed at one point of the neuron morphology. If the neuron is not electrotonically compact, then the membrane is imperfectly clamped far from the voltage clamp electrode.

For example, if the membrane is clamped at a potential V_{clamp} and the neuron is passive (no voltage-dependent ionic channels), then the potential on a dendrite at electrotonic distance d from the soma is $V_0 + (V_{\text{clamp}} - V_0)e^{-d}$, where V_0 is the resting potential (Koch, 1999). Thus, when recording currents (whether synaptic or intrinsic) with somatic voltage clamp, it should be kept in mind that the clamp is imperfect if those currents originate from a distal location. It is difficult to compensate for a poor space clamp (for example by changing the voltage command at the soma), first because the electrotonic distance is generally unknown and second because the potential at the distal location is time-dependent, even with an ideal voltage clamp (the expression above is the stationary value, with passive membrane properties only).

What is the spatial extent of voltage clamping in a neuron? From the expression above, attenuation of the potential is within 10% up to a distance of 5% the electrotonic length of the dendrite, which is given by the following formula:

$$\lambda = \sqrt{\frac{a r_m}{2 r_L}}$$

where a is the radius of the dendrite, r_m is the specific membrane resistance and r_L is the intracellular resistivity. Unfortunately, this analysis only holds when active ionic channels are neglected. When ionic channels open, their conductance increases so that the effective membrane resistance decreases. As a result, the effective electrotonic length decreases, which decreases the spatial extent of voltage clamping. For example, the effective time constant of cortical neurons is about five times smaller *in vivo* than *in vitro* (as assessed by somatic injection of current pulses), presumably because of intense synaptic activity (Destexhe et al., 2003), which increases the total conductance (hence the name *high-conductance state*). If the increase is homogeneous, this conductance increase results in a decrease of electrotonic length by a factor greater than two — or, in other words, the effective size of the neuron doubles. Similarly, intrinsic conductances such as voltage-gated K^+ channels can open with the voltage clamp command, resulting in serious space clamp problems even in small neurons (Bar-Yehuda and Korngreen, 2008).

3.3.2 Double-electrode voltage clamp

In double electrode setups, one electrode is used to measure the membrane potential while the other one is used to inject the feedback current

$I = g(V_{\text{clamp}} - V_m)$. Using two different electrodes ensures that the measure of the membrane potential V_m is not distorted by the injection of the feedback current. This ensures that the membrane potential matches the command clamp potential when the clamp is established (provided junction potentials are properly compensated), because no current passes through the measuring electrode in the stationary regime. Similarly, the measured current in the stationary regime is also correct. However, several factors make the double-electrode voltage clamp non ideal. The most serious problem is capacitive coupling between the two electrodes, which is destabilizing. That coupling limits the gain of the feedback circuit, which results in poorer clamp, longer settling time and distortions in the measured current. Experimentally, capacitive coupling can be reduced by inserting the two electrodes at a wide angle. Unfortunately, it does not suppress all capacitive currents in the recording circuit, in particular the electrode capacitance (through the electrode capillary tube) and the input capacitance (at the amplifier input), which cause similar unstability problems.

To reduce the problems due to capacitances in the recording circuit, voltage clamp amplifiers either introduce a delay in the feedback current or reduce the gain of the feedback. In voltage clamp experiments with a step command potential, the initial transient in the measured current is generally suppressed offline, which makes the measurement of fast activating currents such as sodium channel currents difficult.

3.3.3 Single-electrode voltage clamp

In many cases, it is not possible to insert two electrodes in the neuron and one must use a single electrode to clamp the cell, either a sharp microelectrode or a patch electrode (whole-cell configuration). It introduces an additional problem: the measurement of the membrane potential is contaminated by the injection of the feedback current through the same electrode. There are two kinds of methods to deal with this issue: compensating for the electrode bias (series resistance compensation and AEC) and alternating voltage measurement and current injection (discontinuous voltage clamp).

3.3.3.1 Series resistance compensation

The nature of the problem is similar as in current clamp single-electrode recordings, but the strong feedback makes it more serious. The electrode resistance acts as a voltage divider. In the stationary regime, the command potential and the membrane potential are related by the following relation-

ship:

$$V_m = \frac{R_m}{R_m + R_e} V_{\text{clamp}}$$

where R_m is the membrane resistance and R_e is the electrode resistance (the potentials are relative to the resting potential). Thus, the clamp error increases with R_e. If electrode and membrane resistances have the same magnitude then the error is dramatic, since the membrane potential is only half the command potential. If the electrode resistance is small, the problem might seem minor at first sight, but the electrode resistance results not only in an error on the stationary potential but also in a non-zero settling time and errors on the measured current. Indeed, consider a simple model where the membrane has only passive properties (resistance R_m and capacitance C_m) and the electrode is a resistor (resistance R_e). Applying Kirchhoff's law gives the following differential equation:

$$C_m \frac{dV_m}{dt} + \frac{V_m}{R_m} = \frac{V_{\text{clamp}} - V_m}{R_e}$$

It appears that the membrane potential approaches the stationary voltage exponentially with the following time constant:

$$\tau_{\text{settle}} = \frac{C_m R_m R_e}{R_e + R_m} \approx C_m R_e = \tau_m \frac{R_e}{R_m}$$

where the approximation is valid when $R_e << R_m$. That settling time can be long: for example, if $R_e = R_m/10$ and $\tau_m = 20$ ms, then the stationary clamp error is about 10%, which might be acceptable, but $\tau_{\text{settle}} = 2$ ms, which is long for fast activating channels. This settling time results in a transient in the measured current. Since the measured current is the opposite of the current injected through the electrode, it equals

$$I_{\text{clamp}} = (V_m - V_{\text{clamp}})/R_e$$

Ideally, in our passive neuron model, that measured current should equal the leak current at the command potential, i.e., $-V_{\text{clamp}}/R_m$ (except for an infinite current at onset). With a non zero electrode resistance, the measured current starts at $-V_{\text{clamp}}/R_e$ and relaxes exponentially to $-V_{\text{clamp}}/(R_m + R_e)$ with time constant τ_{settle} (Fig. 3.8A, 0% compensation). Thus, even if the electrode resistance is small, the measured current is completely wrong during the time of the transient (about τ_{settle}). This issue arises even without taking voltage-dependent channels into account, which make the problem much worse. The settling time of the voltage clamp can be shortened by a technique named *supercharging*, which consists in adding a brief pulse

at the onset of a voltage step. Although the membrane potential reaches the target potential quicker, it does not enhance the resolution of the measured currents after the onset. It is important to keep this issue in mind when applying offline series resistance compensation. In many situations, the series resistance cannot be compensated during the recording because of unstability problems (see below), or can only be partially compensated. The electrode resistance R_e can be estimated from the peak of the transient current ($-V_{\text{clamp}}/R_e$; all potentials are relative to the resting potential). The imperfect clamp can then be corrected by applying the following correction to the measured current:

$$I_{\text{corrected}} = I_{\text{measured}} \frac{R_m + R_e}{R_m}$$

if the membrane resistance R_m can be measured. That correction works however only in the stationary regime, when the clamp is established, while the transient current is barely modified.

When recording time-varying currents, the electrode resistance reduces the bandwidth of the measured current, with an approximate cutoff frequency $f_c = 1/(2\pi\tau_{\text{settle}})$, which cannot be corrected by offline compensation (Fig. 3.8B). This filtering property is best understood by considering a simple model of a neuron with a synaptic current $I_s = g_s(t)(E_s - V_m)$. To measure the synaptic conductance, we clamp the neuron at the resting potential (which we choose as the reference potential). The system is governed by the following differential equation:

$$C_m \frac{dV_m}{dt} + g_s(t)(V_m - E_s) + \frac{V_m}{R_m} = -\frac{V_m}{R_e}$$

and the measured current is $-V_m/R_e$, it is proportional to the membrane potential. That equation can be written more clearly as

$$C_m \frac{dV_m}{dt} + g_{\text{tot}}(t)(V_m - E_{\text{eff}}(t)) = 0$$

where $g_{\text{tot}}(t) = g_s(t) + R_m^{-1} + R_e^{-1}$ is the total conductance and

$$E_{\text{eff}}(t) = \frac{g(t)E_s}{g_{\text{tot}}}$$

is the effective reversal potential. The membrane potential follows $E_{\text{eff}}(t)$ with a time constant $C_m/g_{\text{tot}}(t)$, which is close to τ_{settle} if the synaptic conductance is small compared to the electrode conductance R_e^{-1} (if it is not small, then the membrane potential is far from the clamp potential and the recording is probably not useful). In summary, the resolution of current

recordings is about R_e/R_m in units of the membrane time constant, which can be a severe restriction.

It is therefore important to reduce the electrode resistance as much as possible. Correcting the clamp potential by multiplying the clamp potential by $(R_m + R_e)/R_m$ provides similar benefits as offline compensation, i.e., the stationary value is corrected but neither the transient current nor the current filtering are affected. *Series resistance compensation* consists in adding an offset to the command potential that depends on the current injected through the electrode. If I is the current flowing through the electrode (to the neuron) and the electrode is a simple resistor with resistance R_e, then the voltage across the electrode is R_eI. Thus, compensating for the electrode consists in applying a command potential $V_{\text{clamp}} + R_eI$ instead of V_{clamp}. This is in fact the same as bridge balance for current clamp, if one looks at how the feedback current I is implemented: $I = g(V_{\text{clamp}} - U)$, where U is the measured potential and g is the gain of the feedback. Correcting U by bridge balance means changing the feedback current into $I = g(V_{\text{clamp}} - (U - R_eI)) = g(V_{\text{clamp}} + R_eI - U)$, which corresponds to changing the clamp command into $V_{\text{clamp}} + R_eI$. Unfortunately, because I is a feedback current which depends on the measured potential, series resistance compensation is destabilizing. Indeed, with the pure resistor electrode model and an estimated electrode resistance R_e^*, the electrode current reads:

$$I = \frac{V_{\text{clamp}} + R_e^*I - V_m}{R_e}$$

which simplifies to:

$$I = \frac{V_{\text{clamp}} - V_m}{1 - R_e^*/R_e}$$

and that current goes to infinity and changes sign near the ideal setting $R_e^* = R_e$. In fact, the instability point is reached much before that point when considering other capacitances in the circuit such as the electrode capacitance or the amplifier input capacitance (Fig. 3.8A). Thus, series resistance compensation cannot be directly applied in this way. Most amplifiers address this problem by delaying the command offset R_e^*I, which enhances the stability of the system. Even with this strategy, in many cases the electrode resistance can only be partially compensated, especially with high-resistance electrodes. In those cases, an alternative strategy consists of alternating current injection and voltage measurement, in the same way as for discontinuous current clamp.

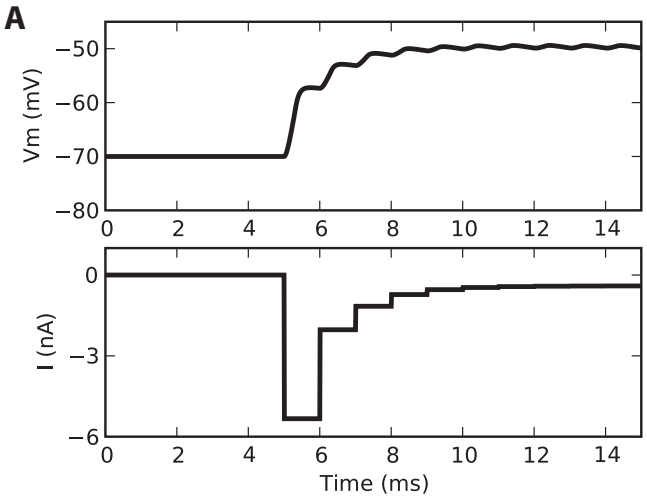

Fig. 3.9. Discontinuous Voltage clamp (numerical simulations). A. The membrane potential of a passive neuron is clamped at -50 mV (from $t = 5$ ms) with discontinuous voltage clamp. The real membrane potential is shown (top) together with the measured current (bottom), which is ideally the constant leak current at -50 mV. The sampling frequency is 1 kHz.

3.3.3.2 Discontinuous voltage clamp

The principle of the discontinuous voltage clamp is identical as the discontinuous current clamp, and works in current clamp mode (the current is imposed, not the voltage). Current injection and potential measurement are alternated so as to minimize the effect of the electrode on the measured potential. Thus, it is subject to the same limitations as DCC: the electrode time constant must be two orders of magnitude smaller than the membrane time constant, and the optimal sampling frequency cannot be determined unambiguously, which results in measurement errors. The principle of the feedback is the same as for continuous voltage clamp, except the current is discretized (Fig. 3.9). During one time step $[t_n, t_{n+1}]$, the injected current is $I_n = g(V_{\text{clamp}} - U(t_n))$, where g is the gain and U is the estimated membrane potential at the end of the previous time step. More precisely, a current $I_n = (g/D)(V_{\text{clamp}} - U(t_n))$ is injected during $[t_n, t_n + D\Delta]$ and current is injected in $[t_n + D\Delta, t_{n+1}]$, where D is the duty cycle (typically about 1/3) and $\Delta = 1/f$ is the sampling step (f is the sampling frequency). It is expected that $V_m(t_n) \approx U(t_n)$, that is, the electrode voltage vanishes at the end of a time step. Under that assumption, the stability of this feedback depends on the size of the sampling step $\Delta = 1/f$ and on the gain

g. Consider that the electrode resistance has indeed been cancelled and that the effective recording circuit consists of a membrane modelled as a resistor and capacitor. Then the membrane potential $V_n = V_m(t_n)$ is governed by the following difference equation:

$$\begin{aligned} V_{n+1} &= e^{-1/\tau_m f} V_n + e^{-(1-D)/\tau_m f}(1 - e^{-D/\tau_m f})\frac{R_m}{D} g(V_{\text{clamp}} - V_n) \\ &\approx (1 - \frac{R_m g}{\tau_m f})V_n + \frac{R_m g}{\tau_m f} V_{\text{clamp}} = (1 - \frac{g}{C_m f})V_n + \frac{g}{C_m f} V_{\text{clamp}} \end{aligned}$$

where we used the fact that $\Delta << \tau_m$ ($\tau_m = R_m C_m$). The gain is optimal when $g = C_m f$ and stable if $g < 2C_m f$. The stationary membrane potential at maximum gain is then:

$$V_m = (1 - \frac{1}{2\tau_m f})V_{\text{clamp}}$$

(after Taylor expansion in $(\tau_m f)^{-1}$). Typically when the frequency is properly adjusted, $\tau_m f \approx 10$, so that the clamp error is about 5% according to the formula above. However a number of factors contribute to raising that error: errors in setting the optimal sampling frequency result in measurement errors, which are a source of instability; non idealities, in particular the electrode capacitance and other capacitances in the circuit, also reduce the maximum gain. The stationary clamp error can be reduced by inserting an additional control current as mentioned in 3.3.1, but it affects neither the settling time nor the resolution of the measured current. Noise is also higher with discontinous voltage clamp, in particular because of aliasing noise in the potential measurement (Finkel and Redman, 1984).

3.3.3.3 Voltage clamp with AEC

Active Electrode Compensation can be used in exactly the same way as discontinous voltage clamp, i.e., the amplifier is in current clamp mode and a feedback current is injected at every time step: $I_n = g(V_{\text{clamp}} - U(t_n))$, where U is the AEC estimation of the membrane potential. The main differences are: 1) the membrane potential is estimated with AEC and 2) the sampling frequency is not limited by the electrode time constant. Therefore the technique is perhaps closer to a continuous voltage clamp with series resistance compensation. An integral control can also be added to the current to improve the quality of the clamp. The AEC-based voltage clamp is still under investigation at this time.

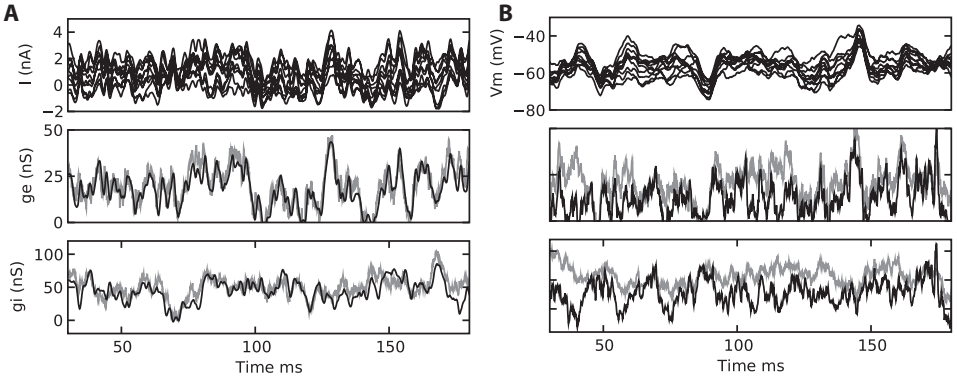

Fig. 3.10. Recording synaptic conductances (numerical simulations with passive neuron model). The neuron model includes a leak current and excitatory and inhibitory noisy synaptic conductances, which are partly reproducible over trials: $g(t) = g_{\text{same}}(t) + g_{\text{different}}(t)$. The reproducible and the variable parts have the same magnitude (i.e., the SNR ratio is 1). A. Measurement of synaptic conductances with voltage clamp (10 different holding potentials; the electrode is 10 MΩ with 90% compensation). Top: measured current (10 trials). Middle: reconstructed excitatory conductance (black) and real one (gray). Bottom: reconstructed inhibitory conductance (black) and real one (gray). B. Current clamp (10 different injected currents; the electrode has negligible resistance). Top: measured membrane potential (10 trials). Middle, bottom: as in A.

3.4 Recording conductances

The earliest recording of the conductance of a neuron is probably the recording of increase in total conductance during action potential performed by Cole and Curtis in 1939 with an ingenious electrical circuit. It proved that the initiation of the action potential was indeed due to an increase in membrane permeability, as was hypothetized by Bernstein. When recording with a current-clamp or voltage-clamp amplifier, conductances can only be inferred indirectly, using a model for the recorded currents or voltages. Conductances can be intrinsic (e.g. conductances of sodium channels) or synaptic, but since we focus on recording neural activity in this chapter, we will mainly discuss the measurement of synaptic conductances.

3.4.1 Models for conductance measurements

3.4.1.1 Current clamp model

Let us start with a simple case where there is only one non-constant conductance in an isopotential neuron. In a current clamp experiment, the membrane potential of that neuron is governed by the following differential

equation:

$$C\frac{dV_m}{dt} = g_l(E_l - V_m) + g(t)(E - V_m) + I(t)$$

where $I(t)$ is the injected current, $g(t)$ is the conductance to be measured and E is the corresponding reversal potential. We assume that E is known. The first term is the leak current, which is assumed to be constant. Such a situation with only one additional current may be obtained by suppressing the expression of other ionic channels with pharmacological methods. In that case the conductance $g(t)$ can be directly derived from the equation:

$$g(t) = (C\frac{dV_m}{dt} - g_l(E_l - V_m) - I(t))/(E - V_m)$$

provided that the parameters C, g_l and E_l are known. These values can be obtained for example from the response of the neuron to a current pulse. It is often easier to suppress the capacitive current by measuring in voltage clamp mode (see below).

Difficulties arise when several time-varying conductances are present:

$$C\frac{dV_m}{dt} = \sum_i g_i(t)(E_i - V_m) + I(t)$$

where $g_i(t)$ is the i^{th} conductance and E_i is the corresponding reversal potential. Ambiguities in the measurement come from the fact that several unknown quantities (the conductances) contribute to the single physical quantity being measured ($V_m(t)$), so that most existing techniques rely on multiple measurements with different injected currents $I(t)$. Since the right hand side is linear with respect to V_m, the equation can be equivalently written as

$$C\frac{dV_m}{dt} = g(t)(E(t) - V_m) + I(t)$$

where

$$g(t) = \sum_i g_i(t)$$

is the total conductance, and

$$E(t) = \frac{\sum_i g_i(t)E_i}{\sum_i g_i(t)}$$

is the effective reversal potential. We observe that the conductances are mapped to the quantities g and gE through a linear mapping $(g_1, g_2, \ldots, g_n) \mapsto (g, gE)$, which is defined by the reversal potentials (which are assumed to be

distinct). That mapping is invertible only if there are no more than two unknown conductances. Otherwise, since the mapping has rank 2, there are an infinite number of linearly related possibilities for the conductances that give the same measurements for the membrane potential and there is no principled way to distinguish between them (except that they must be positive). Besides, even when there are only two time-varying conductances, their values are determined by the choice of the reversal potentials E_i. Thus, for any measurement technique, one can only hope to recover two independent variables at most and their values depend on a choice of reversal potentials, which cannot be inferred from the data. In general, the constant leak current is estimated independently and excitatory and inhibitory conductances are measured. The estimation of the leak current can be obtained for example from the response to pulses during periods of low activity.

There are several issues with the model we described. First, a neuron is not isopotential, which we discuss briefly in section 3.4.1.3. Second, the response of the neuron is nonlinear because of intrinsic voltage-dependent currents (e.g. sodium and potassium currents). That issue can be addressed with more complex models, including polynomial models of the I-V curve or more complex models that can be obtained with white noise injection (Badel et al., 2008). Spike-related conductances (such as those responsible for spike frequency adaptation) can also produce artifacts.

3.4.1.2 Voltage clamp model

In voltage clamp mode, the measured current for an isopotential neuron model reads:

$$I(t) = \sum_i g_i(t)(E_i - V_{\text{clamp}})$$

where V_{clamp} is the holding potential. When there is a single time-varying conductance, it is directly obtained from this formula. When there are several time-varying conductances, the same issues arise as in the current clamp mode. The equation can be rewritten as

$$I(t) = g(t)(E(t) - V_{\text{clamp}})$$

where $g(t)$ is the total conductance and $E(t)$ is the effective reversal potential. Here V_{clamp} is imposed and $I(t)$ is measured. Again, even with many measurements with different holding potentials, only two independent variables can be measured unambiguously, and recovering the values of the conductances depends on the choice of the reversal potentials.

3.4.1.3 Visibility of dendritic synaptic inputs

Two issues arise if the neuron is not electrotonically compact: first, the membrane equation includes a current flowing to the dendrites, second, the currents may be generated distally in the dendrites. In the latter case, there is no direct access to the synaptic conductances if the distance to the dendritic site is large (in units of the space length of the neuron) and one can only talk of "effective" synaptic conductances seen at the soma.

The effect of distal location of synaptic inputs on the measurement is two fold: conductances measured at the soma seem smaller and reversal potentials seem further away from the resting potential. This effect can be understood in a simplified neuron model consisting of an isopotential soma connected to a semi-infinite cylindric dendrite (a "ball-and-stick" model). A synaptic current $g_s(E_s - v)$ is inserted on the dendrite at distance x_s from the soma. We assume for simplicity that the synaptic conductance g_s is constant. A more detailed study can be found in (Koch et al., 1990). We consider a voltage clamp experiment in which the voltage is held fixed at the soma at a value v_0 and the injected current I is measured. According to passive cable theory (Dayan and Abbott, 2001; Tuckwell, 1988), the stationary membrane potential $v(x)$ satisfies the following second order differential equation on the two segments $[0, x_s]$ and $[x_s, +\infty[$:

$$\lambda^2 \frac{d^2 v}{dt} = v$$

where λ is the electrotonic length (we chose the resting potential as the reference potential). The solution of this equation is $v(x) = ae^{x/\lambda} + be^{-x/\lambda}$, where the coefficients a and b must be determined by boundary conditions. At the soma ($x = 0$), the injected current I is the sum of the leak current leaving the membrane and the current flowing through the dendrite:

$$I = g_l v_0 - \frac{1}{R_a} \frac{dv}{dx}(0)$$

where R_a is the axial resistance of the dendrite. At the synaptic site ($x = x_s$), there is a discontinuity in the axial current that equals the synaptic current:

$$-\frac{1}{R_a} \frac{dv}{dx}(x_s^+) = -\frac{1}{R_a} \frac{dv}{dx}(x_s^-) + g_s(E_s - v(x_s))$$

Finally, the membrane potential must vanish at infinity. With these boundary conditions and the continuity at $x = x_s$, one can calculate the potential $v(x)$ over the two segments $[0, x_s]$ and $[x_s, +\infty[$ and ultimately obtain the

current I as a function of v_0 and g_s. After some algebra, we obtain:

$$I(v_0, g_s) = I(v_0, 0) + g^*(v_0 - E^*)$$

where $I(v_0, 0)$ is the effective leak current (current in the absence of synaptic input), g^* is the effective conductance as measured at the soma and E^* the effective reversal potential, which are given by the following expressions:

$$\begin{aligned} E^* &= e^{x_s/\lambda} E_s \\ g^* &= \frac{2g_s}{1 + e^{2x_s/\lambda}} \end{aligned}$$

We observe that $E^* > E_s$ and $g^* < g_s$. The effective reversal potential E^* does not depend on the value of the synaptic conductance g_s. For distal dendrites, the effective reversal potential is further away from the resting potential than the actual reversal potential, and the effective conductance is reduced.

3.4.1.4 Sharp electrodes and patch electrodes

Another important point should be kept in mind: measurements with a sharp microelectrode and with a patch electrode (whole cell configuration) are not equivalent. The main effect of the sharp electrode is to damage the membrane of the cell, which inserts a non-selective leak current. In particular, the leak conductance is larger with a sharp electrode than with a patch electrode. On the other hand, patch electrodes have a large tip which lets the contents of the electrode diffuse in the cell (except with the perforated patch clamp technique, in which antibiotics are used to perforate the membrane). This phenomenon is called *dialysis* and has important consequences. For the measurement of conductances, the main effects are firstly that the resistivity of the intracellular medium is changed (which changes the electrotonic dimension of the neuron) and secondly that synaptic reversal potentials can change over time as the cell is dialyzed (because of changes in ionic concentrations).

3.4.2 Multi-trial conductance measurements

As we noted earlier, when there are several conductances to be measured, ambiguities arise from the fact that only one quantity is measured (the membrane potential in current clamp or the current in voltage clamp). To solve that problem, most current techniques combine measurements on several trials with the same stimulus and different experimental conditions:

different injected currents (current clamp, Fig. 3.10B) or different holding potentials (voltage clamp, Fig. 3.10A). One obvious limitation of this type of technique, which is reviewed in (Monier et al., 2008), is that only stimulus-locked activity can be recorded in this way.

3.4.2.1 Voltage clamp

We start with voltage clamp measurements (Fig. 3.10A). Consider n measurements of the response to the same stimulus, with different holding potentials V_k. Assuming that the synaptic conductances are identical on all trials, the measured current $I_k(t)$ is

$$I_k(t) = g(t)(E(t) - V_k)$$

where $g(t)$ is the total conductance and $E(t)$ is the effective reversal potential. For a given time t, the measure $I_k(t)$ is an affine function of V_k whose slope is the total conductance and intercept is the reversal potential multiplied by the slope. In principle, two trials are sufficient to recover those values but in practice more trials are used to make the measurement more reliable. In that case the conductances are obtained with a linear regression.

Methods based on voltage clamp are mathematically simpler than those based on current clamp because the capacitive current vanishes. However, they raise experimental issues because for practical reasons most intracellular recordings *in vivo* use a single electrode. In many cases, the access resistance cannot be fully compensated, which results in imperfect clamping. If the electrode resistance R_e is known, then the measured current is related to the holding potential V_k according to the following equation:

$$I_k(t) = g(t)(E(t) - V_k + R_e I_k(t))$$

which simplifies to

$$I_k(t) = \frac{g(t)}{1 - g(t)R_e}(E(t) - V_k)$$

and the same linear regression can be applied to recover $g(t)$ and $E(t)$. However, this is only an approximation because the membrane equation should now include a capacitive current, since the membrane potential is not fixed anymore. Other non-idealities such as the input capacitance also make this formula less accurate.

3.4.2.2 Current clamp

Conductance measurements in current clamp mode consist in repeating the same voltage measurements in response to a given stimulus with different

injected currents I_k (Fig. 3.10B). The membrane potential $V_k(t)$ satisfies the following differential equation:

$$I_k - C\frac{dV_k}{dt} = g(t)(V_k(t) - E(t))$$

As in voltage clamp mode, for any given time t, the current $I_k - CdV_k/dt(t)$ is an affine function of $V_k(t)$, whose slope is the total conductance and intercept is the reversal potential multiplied by the slope. Provided that the membrane capacitance C is known (estimated for example from the response to a current pulse), both $g(t)$ and $E(t)$ can be recovered.

This method is experimentally easier than in voltage clamp mode but many other issues arise:

- Differentiating the membrane potential adds noise to the measurements, which may be reduced by filtering.
- Voltage-dependent conductances may be activated. That issue also arises in voltage clamp experiments, but it results in constant biases in the I-V curve, which are easier to compensate for.
- The neuron may fire action potentials. Synaptic conductances cannot be estimated during action potentials because they are masked by the spike-related increase in total conductance (Guillamon et al., 2006). Unfortunately, part of this increase may last for a very long time. For example, pyramidal cortical cells exhibit spike frequency adaptation, related to a slow spike-triggered adaptation conductance whose stationary value increases with the firing rate. Since the firing rate is most likely related to the injected current I_k, the effect on conductance estimation is potentially significant. To avoid this problem, one may pharmacologically block the action potentials or use hyperpolarizing currents.
- Because the membrane potential is not controlled, conductance measurements are less robust to noise in current clamp than in voltage clamp (by noise, we mean any activity that is not locked to the repeated stimulus), as is illustrated by Fig. 3.10.

3.4.3 Statistical measurements

Measuring the time course of synaptic conductances is difficult, either because of technical difficulties (voltage clamp) or because the measurements are not robust to noise (current clamp). A different approach consists in looking for statistical information about the conductances, such as their mean and variance, by using a stochastic model for the neuron and its synaptic inputs. One such model, the "point-conductance" model, consists in a

single-compartment model with time-varying excitatory and inhibitory conductances $g_e(t)$ and $g_i(t)$ described by Ornstein-Uhlenbeck processes (Destexhe et al., 2001), i.e., Gaussian Markov processes with mean g_{e0} (resp. g_{i0}) and standard deviations σ_e (resp. σ_i). That stochastic description derives from a diffusion approximation of the total conductance as a sum of random postsynaptic conductances modelled as exponential functions with time constants τ_e and τ_i. The complete model is described by the following equations:

$$\begin{aligned} C\,\frac{dV_m}{dt} &= -g_l\,(V_m - E_l) - g_e\,(V_m - E_e) - g_i\,(V_m - E_i) + I \\ \frac{dg_e}{dt} &= -\frac{1}{\tau_e}\,[g_e - g_{e0}] + \sqrt{\frac{2\sigma_e^2}{\tau_e}}\;\xi_e(t) \\ \frac{dg_i}{dt} &= -\frac{1}{\tau_i}\,[g_i - g_{i0}] + \sqrt{\frac{2\sigma_i^2}{\tau_i}}\;\xi_i(t) \end{aligned}$$

where C denotes the membrane capacitance, I a stimulation current, g_l the leak conductance, E_l the leak reversal potential, E_e the excitatory reversal potential and E_i the excitatory reversal potential. That model has been used to estimate the distribution of synaptic conductances, synaptic time constants, spike-triggered averages of conductances, and the time course of synaptic conductances.

3.4.3.1 Estimating synaptic conductance distributions

The point-conductance model has been thoroughly studied theoretically and numerically. Different analytic approximations have been proposed to describe the steady-state distribution of the V_m activity of the PC model (Rudolph and Destexhe (2003); Rudolph et al. (2005); Richardson (2004); Lindner and Longtin (2011); for a comparative study, see Rudolph and Destexhe (2011)). One of these expressions can be inverted (Rudolph and Destexhe, 2003; Rudolph et al., 2005), which enables one to directly estimate the synaptic conductance parameters (g_{e0}, g_{i0}, σ_e, σ_i) from experimentally obtained V_m distributions. This constitutes the basis of the VmD method (Rudolph et al., 2004), which we outline below.

The VmD method consists of estimating the statistical properties of the conductances (mean and variance) from the statistics of the intracellularly-recorded activity (mean and variance of the V_m). The following analytic expression provides a good approximation to the steady-state probability distribution $\rho(V_m)$ of the membrane potential (Rudolph and Destexhe, 2003;

Rudolph et al., 2005):

$$\rho(V_m) = N \exp\left[A_1 \ln\left[\frac{u_e(V_m - E_e)^2}{C^2} + \frac{u_i(V_m - E_i)^2}{C^2}\right] + A_2 \arctan\left[\frac{u_e(V_m - E_e) + u_i(V_m - E_i)}{(E_e - E_i)\sqrt{u_e u_i}}\right]\right], \quad (3.3)$$

where $u_e = \sigma_e^2 \tilde{\tau}_e$, $u_i = \sigma_i^2 \tilde{\tau}_i$, A_1 and A_2 are voltage-independent terms depending on the parameters of the membrane equation (see details in Rudolph et al. (2004)). Here, N denotes a normalization constant such that $\int_{-\infty}^{\infty} dV\, \rho(V) = 1$ and $\tilde{\tau}_{\{e,i\}}$ are effective synaptic time constants, given by Rudolph et al. (2005) (see also Richardson (2004)):

$$\tilde{\tau}_{\{e,i\}} = \frac{2\tau_{\{e,i\}}\tilde{\tau}_m}{\tau_{\{e,i\}} + \tilde{\tau}_m}\ , \quad (3.4)$$

where $\tilde{\tau}_m = C/(g_l + g_{e0} + g_{i0})$ is the effective membrane time constant. Due to the multiplicative coupling of the stochastic conductances to the membrane potential, the V_m probability distribution (Eq. 3.3) takes in general an asymmetric form. However, it is well approximated by a Gaussian distribution, which can be obtained by Taylor expansion around the maximum $\bar{V_m}$ of the probability distribution $\rho(V_m)$. The mean and variance of that approximation can be expressed as a function of the parameters (Rudolph et al., 2004). This Gaussian approximation provides an excellent fit to V_m distributions obtained from models and experiments (Rudolph et al., 2004), because the V_m distributions obtained experimentally show little asymmetry (for up-states and activated states; for specific examples, see Rudolph et al. (2004, 2005, 2007); Piwkowska et al. (2008)).

The main advantage of this Gaussian approximation is that it can be easily inverted, which leads to expressions of the synaptic noise parameters as a function of the measured V_m distribution, specifically $\bar{V_m}$ and σ_V. By fixing the values of τ_e and τ_i, which are related to the decay time of synaptic currents and can be estimated from voltage-clamp data and/or current-clamp by using power spectral analysis (see below), four parameters remain to be estimated: the means (g_{e0}, g_{i0}) and standard deviations (σ_e, σ_i) of excitatory and inhibitory synaptic conductances. Since the Gaussian distribution is only characterized by two values ($\bar{V_m}$ and σ_V), at least two recordings with different constant levels of injected current I are required, as for multitrial conductance measurements (Rudolph et al., 2004). The quality of the estimation can then be assessed by comparing the full expression (Eq 3.3) with the experimental data.

These relations enable us to estimate global characteristics of network activity, such as mean excitatory (g_{e0}) and inhibitory (g_{i0}) synaptic conductances, as well as their respective variances (σ_e^2, σ_i^2), from the sole knowledge of the V_m distributions computed from intracellular measurements. This VmD method has been tested using computational models (Fig. 3.11A) and dynamic-clamp experiments (Fig. 3.11B-C; Rudolph et al. (2004); Piwkowska et al. (2008)) and has also been used to extract conductances from different experimental conditions *in vivo* (Rudolph et al., 2005, 2007; Zou et al., 2005). In particular, it was applied to analyze intracellular recordings in anesthetized (Rudolph et al., 2005), as well as naturally sleeping and awake cats (Rudolph et al., 2007).

3.4.3.2 Estimating synaptic time constants from the power spectrum

Synaptic time constants (τ_e and τ_i) can be estimated from the power spectral density (PSD) of the membrane potential, which, for the point-conductance model, can be well approximated by the following expression (Destexhe and Rudolph, 2004):

$$S_V(\omega) \;=\; \frac{4}{G_T^2}\;\frac{1}{1+\omega^2\;\tilde{\tau}_m^2}\;\left[\frac{\sigma_e^2\tau_e\;(E_e-\bar{V})^2}{1+\omega^2\;\tau_e^2}\;+\;\frac{\sigma_i^2\tau_i\;(E_i-\bar{V})^2}{1+\omega^2\;\tau_i^2}\right]\;, \quad (3.5)$$

where $\omega = 2\pi f$, f is the frequency, $G_T = g_L + g_{e0} + g_{i0}$ is the total membrane conductance, $\tilde{\tau}_m = C/G_T$ is the effective time constant, and $\bar{V} = (g_L E_L + g_{e0} E_e + g_{i0} E_i)/G_T$ is the average membrane potential. The "effective leak" approximation used to derive this equation consisted in incorporating the average synaptic conductances into the total leak conductance, and then considering that fluctuations around the obtained mean voltage are subjected to a constant driving force (Destexhe and Rudolph, 2004).

That expression is very accurate for single-compartment models and provides an excellent fit for neurons stimulated with dynamic clamp *in vitro* up to frequencies of about 500 Hz, above which the mismatch was presumably due to instrumental noise (Piwkowska et al., 2008). However, the fit with *in vivo* recordings is more approximate for frequencies above 100 Hz (Rudolph et al., 2005), where the PSD scales as $1/f^{2.5}$ instead of $1/f^4$. This different scaling may be due to the attenuation of synaptic inputs occurring on dendrites, as well as to the non-ideal aspect of the membrane capacitance (Bédard and Destexhe, 2008). Nevertheless, the matching of the expression above to the low-frequency end (<100 Hz) of the PSD yielded values of time constants of $\tau_e = 3$ ms and $\tau_i = 10$ ms, with a precision of the order of 30 % (Rudolph et al., 2005).

3.4.3.3 Estimating spike-triggered average conductances

The VmD method can be used to extract the spike-triggered averages (STAs) of conductances from recordings of the V_m (Pospischil et al., 2007). The basis of the STA method is to, first, calculate the STA of the V_m activity, and then search for the "most likely" spike-related conductance time courses ($g_e(t)$, $g_i(t)$) that are compatible with the observed voltage STA. Assuming that both conductances are realizations of Ornstein-Uhlenbeck processes whose means (g_{e0},g_{i0}) and variances (σ_e^2, σ_i^2) are known (estimated with the VmD method), the probability of a given conductance time course $(g_e(t), g_i(t))$ can be calculated from the definition of the stochastic processes. Because Ornstein-Uhlenbeck processes are Gaussian Markov processes, the probability of $(g_e(t+dt), g_i(t+dt))$ only depends on the value $(g_e(t), g_i(t))$ and is normally distributed. It follows that, if time is discretized, the log of the probability of a given conductance time course is a sum of quadratic terms, so that the maximum likelihood solution can be found with linear algebra (Pospischil et al., 2007).

The STA method predicted the correct results in numerical simulations and *in vitro* using dynamic clamp injection of known patterns in real neurons (Pospischil et al., 2007). It was also applied to intracellular recordings in awake and naturally sleeping cats (Rudolph et al., 2007), where it was found that for the majority of neurons, spikes are correlated with a decrease of inhibitory conductance, suggesting that inhibition is most effective in determining spiking activity. This observation matches the dominance of inhibition observed using the VmD method in the same neurons (see above).

3.4.3.4 Estimating the time course of synaptic conductances

The two different strategies outlined above, the VmD and STA methods, can be merged into a new method. The method, called "VmT", extracts synaptic conductance parameters, similar to the VmD method, but using a maximum-likelihood estimation similar to the STA method, thus applicable to single V_m traces (Pospischil et al., 2009). By following a similar procedure as for the STA method, one obtains estimates of the "most likely" values for g_{e0}, g_{i0}, σ_e and σ_i from single V_m traces. Similar to above, the method was tested using computational models and dynamic-clamp experiments; the VmT methods performs remarkably well for high-conductance states (see details in Pospischil et al. (2009)).

3.5 Conclusion

Intracellular electrophysiology is one of the oldest technique for measuring neural activity. There are essentially two recording modes: current clamp, in which the membrane potential is measured, and voltage clamp, in which currents are measured while the membrane potential is held fixed. Conductance measurements are based on those two recording modes. Most of the experimental difficulties come from two unavoidable aspects: firstly, the non-ideality of the electrode biases the measurements and causes stability problems; secondly, current can only be injected at a single point of the cell, which makes it difficult to control the potential at distal sites in the neuron.

Although electrodes and amplifiers are well established experimental devices, we might expect new developments in measuring techniques in the future, either in the way recordings are analyzed or in the way the experimental devices are controlled. We list below a few areas where new techniques might emerge in the future:

- recording techniques using numerical models of neurons and/or of the experimental apparatus (e.g. electrodes), as were introduced recently for current clamp and dynamic clamp recordings (Brette et al., 2008);
- dynamic clamp techniques: dynamic clamp recordings consist in injecting a current that depends in real time on the measured potential, which poses specific technical problems (Brette et al., 2009);
- single-trial conductance measurements: model-based and/or statistical techniques could be used to estimate the time course of synaptic conductances in single trials.

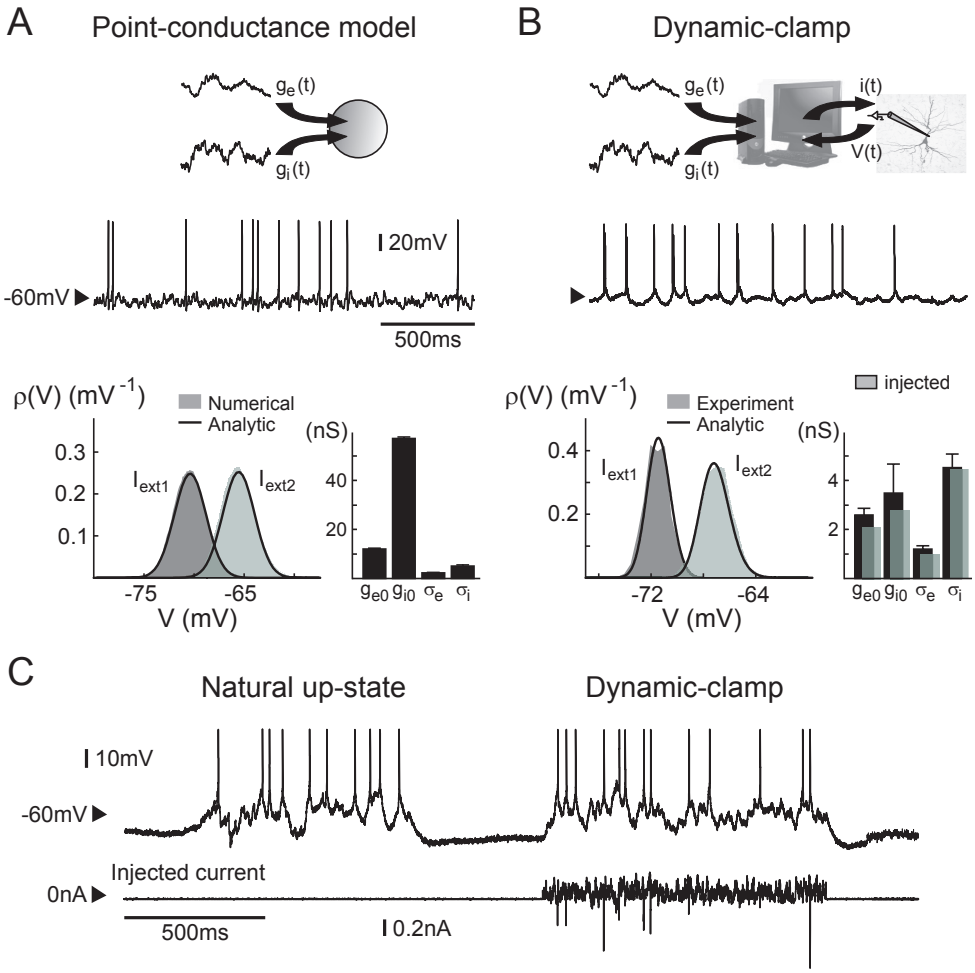

Fig. 3.11. Numerical and dynamic-clamp test of the VmD method to extract conductances. A. Simulation of the point-conductance model (top trace) and comparison between numerically computed V_m distributions (bottom; left) and the analytic expression (black; conductance values shown in the bar graph). B. Dynamic-clamp injection of the point-conductance model in a real neuron. (Right) Conductance parameters are re-estimated (black bars; error bars are standard deviations obtained when the same injected conductance parameters are re-estimated in different cells) from the V_m distributions and compared to the known parameters of the injected conductances (grey bars). (Left) The experimental V_m distributions are compared to the analytic distributions calculated using the re-estimated conductance parameters. C. Comparison of a spontaneous up-state (Natural up-state) with an artificial up-state recreated using conductance injection (Dynamic-clamp). Modified from Rudolph et al. (2004).

Numerical simulations

All numerical simulations were done using the Brian simulator (Goodman and Brette, 2008), which is freely available at `http://www.briansimulator.org`. The scripts for the figures can be downloaded at `http://www.briansimulator.org/electrophysiology`. All neuron models were single-compartment models, with either passive properties (Figures 3.4, 3.6, 3.8, 3.9, 3.10) or ionic channels with Hodgkin-Huxley type dynamics (Figures 3.3, 3.5), adapted from (Mainen et al., 1995). Synaptic activity (Figures 3.8, 3.5, 3.10) was modelled as fluctuating excitatory and inhibitory conductances represented by halfwave rectified Ornstein-Uhlenbeck processes. Electrodes were modelled as RC circuits or two RC circuits in series. Amplifier models include bridge balance, capacitance neutralization, discontinuous current clamp and voltage clamp.

References

Anderson, J., Carandini, M., and Ferster, D. (2000). Orientation tuning of input conductance, excitation, and inhibition in cat primary visual cortex. *J neurophysiol*, 84(2):909.

Azouz, R. and Gray, C. M. (1999). Cellular mechanisms contributing to response variability of cortical neurons in vivo. *J Neurosci*, 19(6):2209–23.

Badel, L., Lefort, S., Brette, R., Petersen, C. C. H., Gerstner, W., and Richardson, M. J. E. (2008). Dynamic I-V curves are reliable predictors of naturalistic pyramidal-neuron voltage traces. *Journal of Neurophysiology*, 99(2):656–66.

Bal, T. and McCormick, D. A. (1996). What stops synchronized thalamocortical oscillations? *Neuron*, 17(2):297.

Bar-Yehuda, D. and Korngreen, A. (2008). Space-Clamp problems when voltage clamping neurons expressing Voltage-Gated conductances. *J Neurophysiol*, 99(3):1127–1136.

Bédard, C. and Destexhe, A. (2008). A modified cable formalism for modeling neuronal membranes at high frequencies. *Biophysical Journal*, 94(4):1133–1143.

Bernstein, J. (1868). Ueber den zeitlichen verlauf der negativen schwankung des nervenstroms. *Pflügers Archiv European Journal of Physiology*, 1(1):173–207.

Bernstein, J. (1912). *Elektrobiologie*. Die Wissenschaft,, 44 Hft, Wissenschaft, Braunschweig.

Borg-Graham, L. J., Monier, C., and Fregnac, Y. (1998). Visual input evokes transient and strong shunting inhibition in visual cortical neurons. *Nature*, 393(6683):369.

Brennecke, R. and Lindemann, B. (1971). A chopped-current clamp for current injection and recording of membrane polarization with single electrodes of changing resistance. *TI-TJ Life Sci*, 1:53–58.

Brennecke, R. and Lindemann, B. (1974). Design of a fast voltage clamp for biological membranes, using discontinuous feedback. *Rev Sci Instrum*, 45(5):656–61.

Brette, R., Piwkowska, Z., Monier, C., Francisco, J., Gonzalez, G., Frégnac, Y., Bal,

T., and Destexhe, A. (2009). *Dynamic Clamp with High-Resistance Electrodes Using Active Electrode Compensation In Vitro and In Vivo*, pages 1–36.

Brette, R., Piwkowska, Z., Monier, C., Rudolph-Lilith, M., Fournier, J., Levy, M., Frgnac, Y., Bal, T., and Destexhe, A. (2008). High-resolution intracellular recordings using a real-time computational model of the electrode. *Neuron*, 59(3):379–91.

Brock, L., Coombs, J., and Eccles, J. (1952). The recording of potentials from motoneurones with an intracellular electrode. *The Journal of Physiology*, 117(4):431–460.

Cole, K. S. (1949). Dynamic electrical characteristics of the squid axon membrane. *Arch. Sci. Physiol*, 3(25):3–25.

Cole, K. S. and Curtis, H. J. (1939). Electric impedance of the squid giant axon during activity. *The Journal of General Physiology*, 22(5):649–670.

Dayan, P. and Abbott, L. F. (2001). *Theoretical neuroscience*. MIT Press Cambridge, Mass.

de Polavieja, G. G., Harsch, A., Kleppe, I., Robinson, H. P. C., and Juusola, M. (2005). Stimulus history reliably shapes action potential waveforms of cortical neurons. *Journal of Neuroscience*, 25(23):5657–5665.

de Sa, V. R. and MacKay, D. J. (2001). Model fitting as an aid to bridge balancing in neuronal recording. *Neurocomputing*, 38-40:1651–1656.

Destexhe, A. and Rudolph, M. (2004). Extracting information from the power spectrum of synaptic noise. *Journal of Computational Neuroscience*, 17(3):327–345.

Destexhe, A., Rudolph, M., Fellous, J. M., and Sejnowski, T. J. (2001). Fluctuating synaptic conductances recreate in vivo-like activity in neocortical neurons. *Neuroscience*, 107(1):13.

Destexhe, A., Rudolph, M., and Pare, D. (2003). The high-conductance state of neocortical neurons in vivo. *Nat Rev Neurosci*, 4(9):739.

DeWeese, M. R., Wehr, M., and Zador, A. M. (2003). Binary spiking in auditory cortex. *The Journal of Neuroscience: The Official Journal of the Society for Neuroscience*, 23(21):7940–9.

Engel, A. K., Fries, P., and Singer, W. (2001). Dynamic predictions: oscillations and synchrony in top-down processing. *Nat Rev Neurosci*, 2(10):704.

Finkel, A. S. and Redman, S. (1984). Theory and operation of a single microelectrode voltage clamp. *J Neurosci Methods*, 11(2):101–27.

Galvani, L. (1791). De viribus electricitatis in motu musculari: Commentarius. *Bologna: Tip. Istituto delle Scienze, 1791; 58 p.: 4 tavv. ft; in 4.; DCC. f. 70.*

Goodman, D. and Brette, R. (2008). Brian: a simulator for spiking neural networks in python. *Frontiers in Neuroinformatics*, 2:5.

Guillamon, A., McLaughlin, D. W., and Rinzel, J. (2006). Estimation of synaptic conductances. *Journal of Physiology-Paris*, 100(1-3):31–42.

Henze, D. A. and Buzsaki, G. (2001). Action potential threshold of hippocampal pyramidal cells in vivo is increased by recent spiking activity. *Neuroscience*, 105(1):121–30.

Hille, B. (2001). *Ion Channels of Excitable Membranes*. Sinauer Associates.

Hodgkin, A. and Huxley, A. (1939). Action potentials recorded from inside a nerve fibre. *Nature*, 144(3651):710.

Hodgkin, A. and Huxley, A. (1952). A quantitative description of membrane current and its application to conduction and excitation in nerve. *J physiol (lond)*, 117:500.

Hodgkin, A. L. and Katz, B. (1949). The effect of sodium ions on the electrical activity of the giant axon of the squid. *The Journal of Physiology*, 108(1):37.

Koch, C. (1999). *Biophysics of computation: Information processing in single neurons*. Oxford University Press, USA.

Koch, C., Douglas, R., and Wehmeier, U. (1990). Visibility of synaptically induced conductance changes: theory and simulations of anatomically characterized cortical pyramidal cells. *The Journal of Neuroscience*, 10(6):1728 –1744.

Lampl, I., Reichova, I., and Ferster, D. (1999). Synchronous membrane potential fluctuations in neurons of the cat visual cortex. *Neuron*, 22(2):361.

Leger, J. F., Stern, E. A., Aertsen, A., and Heck, D. (2005). Synaptic integration in rat frontal cortex shaped by network activity. *J Neurophysiol*, 93(1):281–93.

Lindner, B. and Longtin, A. (2011). Comment on "Characterization of subthreshold voltage fluctuations in neuronal membranes," by m. rudolph and a. destexhe. *Neural Computation*, 18(8):1896–1931.

Ling, G. and Gerard, R. (1949). The normal membrane potential of frog sartorius fibers. *Journal of Cellular Physiology*, 34(3):383–96.

Mainen, Z. and Sejnowski, T. (1995). Reliability of spike timing in neocortical neurons. *Science*, 268:1503.

Mainen, Z. F., Joerges, J., Huguenard, J. R., and Sejnowski, T. J. (1995). A model of spike initiation in neocortical pyramidal neurons. *Neuron*, 15(6):1427–1439.

Marmont, G. (1949). Studies on the axon membrane; a new method. *J Cell Physiol*, 34(3):351–82.

Monier, C., Chavane, F., Baudot, P., Graham, L. J., and Fregnac, Y. (2003). Orientation and direction selectivity of synaptic inputs in visual cortical neurons: a diversity of combinations produces spike tuning. *Neuron*, 37(4):663.

Monier, C., Fournier, J., and Fregnac, Y. (2008). In vitro and in vivo measures of evoked excitatory and inhibitory conductance dynamics in sensory cortices. *Journal of Neuroscience Methods*, In Press, Corrected Proof(2):323–365.

Neher, E. and Sakmann, B. (1976). Single-channel currents recorded from membrane of denervated frog muscle fibres. *Nature*, 260(5554):799–802.

Pare, D., Shink, E., Gaudreau, H., Destexhe, A., and Lang, E. J. (1998). Impact of spontaneous synaptic activity on the resting properties of cat neocortical pyramidal neurons in vivo. *J neurophysiol*, 79(3):1450.

Piwkowska, Z., Pospischil, M., Brette, R., Sliwa, J., Rudolph-Lilith, M., Bal, T., and Destexhe, A. (2008). Characterizing synaptic conductance fluctuations in cortical neurons and their influence on spike generation. *Journal of Neuroscience Methods*, 169(2):302–22.

Pospischil, M., Piwkowska, Z., Bal, T., and Destexhe, A. (2009). Extracting synaptic conductances from single membrane potential traces. *Neuroscience*, 158(2):545–552.

Pospischil, M., Piwkowska, Z., Rudolph, M., Bal, T., and Destexhe, A. (2007). Calculating Event-Triggered average synaptic conductances from the membrane potential. *Journal of Neurophysiology*, 97(3):2544.

Purves, R. D. (1981). *Microelectrode methods for intracellular recording and ionophoresis*. Academic Press New York.

Richardson, M. J. E. (2004). Effects of synaptic conductance on the voltage distribution and firing rate of spiking neurons. *Physical Review E*, 69(5):051918.

Rudolph, M. and Destexhe, A. (2003). Characterization of subthreshold voltage fluctuations in neuronal membranes. *Neural Comput*, 15(11):2577.

Rudolph, M. and Destexhe, A. (2011). On the use of analytical expressions for the

voltage distribution to analyze intracellular recordings. *Neural Computation*, 18(12):2917–2922.

Rudolph, M., Pelletier, J. G., Paré, D., and Destexhe, A. (2005). Characterization of synaptic conductances and integrative properties during electrically induced EEG-Activated states in neocortical neurons in vivo. *Journal of Neurophysiology*, 94(4):2805 –2821.

Rudolph, M., Piwkowska, Z., Badoual, M., Bal, T., and Destexhe, A. (2004). A method to estimate synaptic conductances from membrane potential fluctuations. *Journal of Neurophysiology*, 91(6):2884–2896.

Rudolph, M., Pospischil, M., Timofeev, I., and Destexhe, A. (2007). Inhibition determines membrane potential dynamics and controls action potential generation in awake and sleeping cat cortex. *The Journal of Neuroscience*, 27(20):5280 –5290.

Sakmann, B. and Neher, E. (1995). *Single-channel recording*. Plenum Press New York.

Sherman-Gold, R. (1993). *The axon guide for electrophysiology and biophysics: laboratory techniques*. Axon Instruments Foster City, CA.

Sigworth, F. J. and Neher, E. (1980). Single na channel currents observed in cultured rat muscle cells. *Nature*, 287(2):447.

Staley, K. J., Otis, T. S., and Mody, I. (1992). Membrane properties of dentate gyrus granule cells: comparison of sharp microelectrode and whole-cell recordings. *J Neurophysiol*, 67(5):1346–1358.

Stuart, G., Spruston, N., and Hausser, M. (1999). *Dendrites*. Oxford University Press, USA.

Tuckwell, H. (1988). *Introduction to theoretical neurobiology, vol 1: linear cable theory and dendritic structure*. Cambridge University Press, Cambridge.

Umrath, K. (1930). Untersuchungen über plasma und plasmaströmung an characeen. *Protoplasma*, 9(1):576–597.

Volgushev, M., Pernberg, J., and Eysel, U. (2002). A novel mechanism of response selectivity of neurons in cat visual cortex. *J physiol*, 540(Pt 1):307.

Wilent, W. B. and Contreras, D. (2005). Stimulus-dependent changes in spike threshold enhance feature selectivity in rat barrel cortex neurons. *J Neurosci*, 25(11):2983–91.

Zou, Q., Rudolph, M., Roy, N., Sanchez-Vives, M., Contreras, D., and Destexhe, A. (2005). Reconstructing synaptic background activity from conductance measurements in vivo. *Neurocomputing*, 65-66:673–678.